Time and Duration of Chondrule Formation: Constraints from ^{26}Al-^{26}Mg Ages of Individual Chondrules

J. Pape[1,*]

K. Mezger[1]

A.-S. Bouvier[2]

L. P. Baumgartner[2]

[1] Institute of Geological Sciences, University of Bern, Baltzerstrasse 1+3, CH-3012 Bern, Switzerland

[2] Institute of Earth Sciences, University of Lausanne, UNIL-Mouline, CH-1015 Lausanne, Switzerland

* Corresponding author: jonas.pape@geo.unibe.ch

Original paper submitted to *Geochimica et Cosmochimica Acta*

Keywords: chondrule formation, ^{26}Al-^{26}Mg chronology, initial $^{26}Al/^{27}Al$, SIMS, early solar system chronology, unequilibrated ordinary chondrites

Abstract

Chondrules from unequilibrated ordinary and carbonaceous chondrites belong to the oldest and most primitive materials from the early solar system and record chemical and isotopic signatures relating to their formation and evolution. These signatures allow tracing protoplanetary disk processes that eventually led to the formation of planetary building blocks and rocky planets. ^{26}Al-^{26}Mg ages based on mineral-mesostasis isochrons of 31 porphyritic ferromagnesian chondrules, that belong mainly to type-II, constrain the time of chondrule melting prior to incorporation into the respective chondrite parent bodies. For this study chondrules from the unequilibrated L, L(LL) and LL ordinary chondrites (UOCs) NWA 5206, NWA 8276, MET 96503, MET 00452, MET 00526, NWA 7936 and QUE 97008 were selected, which are of petrologic types 3.00 to 3.15 and were thus least metamorphosed after formation. Magnesium and Al isotopes were measured in-situ by Secondary Ion Mass Spectrometry (SIMS) using a CAMECA 1280 ims. ^{26}Mg excess from in-situ decay of ^{26}Al correlating with $^{27}Al/^{24}Mg$ has been detected in the mesostasis of all but one chondrule. The initial Al isotopic compositions $(^{26}Al/^{27}Al)_0$ and $^{26}Mg/^{24}Mg$ ratios ($\delta^{26}Mg^*_0$) deduced from internal mineral isochron regressions range from $(9.5 \pm 2.8) \times 10^{-6}$ to $(3.1 \pm 1.2) \times 10^{-6}$ and $-0.020 \pm 0.028‰$ to $0.011 \pm 0.039‰$, respectively. The corresponding chondrule ages (Δt_{CAI}), calculated relative to calcium-aluminum-rich inclusions (CAIs) using the canonical $^{26}Al/^{27}Al = (5.23 \pm 0.13) \times 10^{-5}$, are between $1.76^{+0.36}_{-0.27}$ and $2.92^{+0.51}_{-0.34}$ Ma and date melt formation and thus ~~the~~ primary chondrule formation from dust-like precursors or reprocessing of older chondrules. The age range agrees with those acquired with different short-lived chronometers and with published ^{26}Al-^{26}Mg ages, the majority of which were obtained for chondrules from the Bishunpur and Semarkona meteorites, although no chondrule with $(^{26}Al/^{27}Al)_0 > 10^{-5}$ was found.

Chondrules in single chondrite samples or between different chondrite groups show no distinct age distributions. The initial $^{26}Al/^{27}Al$ of the oldest chondrules in the L(LL)/LL and L chondrite samples are identical within their 1σ uncertainties and yield a mean age of $1.99^{+0.08}_{-0.08}$ Ma and $1.81^{+0.11}_{-0.10}$ Ma, respectively. The oldest chondrules from six of the seven studied samples record a mean age of $1.94^{+0.07}_{-0.06}$ Ma. Since heating events in the protoplanetary disk could have partially reset the Al-Mg systematics in pre-existing chondrules and this would have shifted recorded ^{26}Al-^{26}Mg ages toward younger dates, the oldest mean age of $1.81^{+0.11}_{-0.10}$ Ma recorded in L chondrite chondrules is interpreted to date the rapid and punctuated onset of chondrule formation. The density distribution of chondrule ages from this study, which comprises the largest single dataset of OC chondrule ages, combined with published ages for chondrules from ordinary and carbonaceous chondrites reveals major age peaks for OC chondrules at 2.0 and 2.3 Ma. Chondrules in ordinary and carbonaceous chondrites formed almost contemporaneously (with a possible distinction between CC groups) in two chemically distinct reservoirs, probably in density-enriched regions at the edges of Jupiter's orbit. The young formation ages of chondrules suggest that they do not represent precursors but rather by-products of planetesimal accretion.

1. Introduction

Unequilibrated ordinary and carbonaceous chondrites (UOC and CC) and their major components chondrules, matrix and the oldest solar system solids calcium-aluminum-rich inclusions (CAIs), preserve mineralogical, chemical and isotopic information on early solar system processes from first formation of solids to their incorporation into planetesimals. Chondrites rank among the chemically most primitive objects in the solar system and contain, with the exception of CI meteorites, between 20 and 80 vol% chondrules (Weisberg et al., 2006), that represent partially crystallised melt droplets. Chondrites were always considered as potential precursors from which the terrestrial planets formed (e.g. Wasson and Kallemeyn 1988, Johansen et al., 2015). However, the process that led to chondrule formation and the absolute time when this process actually occurred in the protoplanetary disk (PPD) are controversially debated and remain among the most discussed and ambiguous issues in the fields of meteoritics and early solar system science.

Proposed chondrule forming processes are broadly divided into nebular and planetary formation models. The first model places chondrule formation in the PPD where they formed from precursor material like dust agglomerates by brief heating events to form first generation chondrules that may have been remelted during subsequent heating episodes. Solar nebular lightning (e.g. Desch and Cuzzi, 2000), gravitational instabilities (e.g. Youdin and Shu, 2002) and shock processing of dust, referred to as bow shocks around planetary embryos (e.g. Morris et al., 2012) could have supplied sufficient energy to melt chondrules in such a scenario. In the planetary formation model, chondrules are formed during planetesimal collisions (e.g. Asphaug et al., 2011; Lichtenberg et al., 2018) and a similar process is widely accepted to have resulted in the formation of young, unusual chondrules as found in the CB Gujba meteorite (Krot et al., 2005).

Any consistent model of chondrule formation must account for major geochemical and textural observations in chondrites and chondrules, like (i) high peak temperatures of ~1500-1800 °C required to reach liquidus of mafic phases (Hewins and Connolly, 1996), (ii) cooling rates in the range of ~10-1000 K h^{-1} (Desch and Connolly, 2002), (iii) likely elevated alkali vapour pressure to prevent K isotope fractionation during chondrule formation (Alexander et al., 2000), (iv) evidence of chondrule reworking at high temperatures (e.g. presence of relict grains), (v) complementarity of refractory elements (Hezel and Palme, 2010; Palme et al., 2015) and Mo isotopes between chondrules and matrix (Budde at al., 2016).

Another key component towards a consistent early solar system evolution model (resulting in planetesimals and eventually planets) is a precise chronology that constrains the timeline of chondrule formation and the question whether chondrules formed early and potentially served as building blocks of the rocky planets or formed late, possibly as by-products of planetesimal formation. Common isotope systems applied to determine chondrule ages are the long-lived, absolute Pb-Pb (e.g. Amelin et al., 2002; Bollard et al., 2017; Connelly et al., 2017; and references therein) and the short-lived ^{53}Mn-^{53}Cr (e.g. Yin et al., 2007), ^{182}Hf-^{182}W (e.g. Becker et al., 2015; Budde et al., 2016) and ^{26}Al-^{26}Mg (e.g. Kita et al., 2000; Rudraswami and Goswami, 2007; Villeneuve et al., 2009; Kita and Ushikubo, 2012 and references therein) chronometers, of which the latter theoretically provides the best age resolution due to the short half-life of ^{26}Al (0.717 Ma, National Nuclear Data Center NuDat v2.7, 2018) and its initially high abundance. Chronometry with the ^{26}Al-^{26}Mg decay scheme relies on the assumption that ^{26}Al was homogeneously distributed in the reservoir from which chondrules formed. Bulk ^{26}Al isochrons constructed from Allende CAIs (so-called *canonical* ^{26}Al/^{27}Al = (5.23 ± 0.13) × 10^{-5}, Jacobsen et al., 2008) or Efremovka CAIs-AOAs (^{26}Al/^{27}Al = (5.252 ± 0.019) × 10^{-5}, Larsen et al., 2011) are generally accepted to define the abundance of ^{26}Al in the innermost region of the PPD at the time of CAI formation which is equated with the time of first formation of solids. This canonical abundance of ^{26}Al is commonly used to define the time anchor for relative ^{26}Al-^{26}Mg mineral isochron dating. Mineral ^{26}Al-^{26}Mg isochrons from Type B CAIs record a slightly lower initial Al isotopic composition $(^{26}Al/^{27}Al)_0$ ~5×10^{-5} that is interpreted to reflect processing and crystallization of CAI components shortly after formation of their precursors from the solar nebular gas (MacPherson et al., 1995; Kita et al., 2012). The basic assumption of a homogeneous distribution of ^{26}Al throughout the inner parts of the PPD is subject to current research (e.g. Larsen et al., 2011; Schiller et al., 2015; Larsen et al., 2016). This issue is discussed and evaluated in section *5.1*.

Most published ^{26}Al-^{26}Mg ages of single chondrules, based on the canonical value, range from ~1.8 to 3.0 Ma after CAIs with only a few chondrules showing older or younger ages (e.g. Villeneuve et al., 2009; Kita and Ushikubo 2012). However, the majority of OC chondrule dates were acquired from only two LL-chondrites, the Semarkona and Bishunpur meteorites. Systematic age differences for magnesian type-I (Mg#>90) and ferroan type-II (Mg#<90) chondrules, for which a genetic and chronological relationship is discussed (e.g. Jones et al., 2005; Villeneuve et al., 2015), are ambiguous. Age distributions between different chondrite samples and types do not show clear trends. ^{26}Al-^{26}Mg ages of chondrules from UOCs and most

CCs peak between 2.0 and 2.5 Ma after CAIs. The onset of chondrule formation in CCs may slightly postdate formation of chondrules in ordinary chondrites (Kurahashi et al., 2008; Villeneuve et al., 2009). The general age range obtained by ^{26}Al-^{26}Mg chronology seems to be confirmed by most other chronological isotope systems. Pb-Pb dates from two recent studies (Connelly et al., 2012; Bollard et al., 2017) are in apparent conflict with the late formation of chondrules and propose chondrule formation starting contemporaneously with CAI and continuing for about 4 Myr. Generally, published chondrule age data are discussed controversially with a lively debate on their meaning and significance for early solar system chronology.

Chondrules from primitive, unequilibrated chondrites of petrologic type 3.00-3.15 were not heated sufficiently to initiate significant metamorphic overprint and equilibration on the parent bodies and thus preserve some of the most primitive and unprocessed material from the early solar system. They are best suited to study the chronology of last melting and crystallisation of chondrules. Even though considered primitive, chemical and textural evidence like magnesian relict grains in ferroan chondrules, disproportionately large phenocrysts, unusual compositional zoning, complex overgrowth of olivine and pyroxene phenocrysts and igneous rims, suggest that some chondrules experienced re-heating and (at least) partial re-melting after primary formation (e.g. Wasson and Rubin, 2003; Rubin 2010). Quick and rapid subsequent cooling of chondrules following the heating and last melting event might have ensured closed systems, as it was recently suggested for some Type-II chondrules from Semarkona (Baecker et al., 2017).

Recent technical advances like large geometry Secondary Ion Mass Spectrometry (SIMS) and a greater attention to analytical aspects like fractionation correction have resulted in higher-precision Mg isotope analyses, that significantly improved the resolution of the ^{26}Al-^{26}Mg chronometer and make it now possible to obtain precise ages for materials with relatively low Al/Mg ratios, such as individual chondrules and their components. In this study, Mg and Al isotope analyses were performed on olivine, pyroxene and glassy mesostasis in 31 least metamorphosed chondrules (Fig. 1, Fig. S1, S2). The measurements for the broad set of chondrules from seven unequilibrated L, L(LL) and LL ordinary chondrites presented here increases the number of high precision ^{26}Al-^{26}Mg ages for OC chondrules obtained in the course of a single study using an identical analytical set up. These specimens were selected, because ordinary chondrites sample an isotopic reservoir that is likely distinct from carbonaceous chondrites and more similar to the reservoir from which also enstatite chondrites and the terrestrial planets formed (Warren, 2011; Budde et al., 2016). This makes them especially suited study objects in the persistent discussion on the role of chondrules in the evolution of the rocky planets.

The data presented here add a significant number of chondrule ages to the published data sets and are discussed in the context of chondrite and chondrule types, compared with previously published Pb-Pb and ^{26}Al-^{26}Mg ages and provide constraints on the beginning and duration of chondrule formation in the early solar system.

2. Methods

2.1 Secondary ion mass spectrometry (SIMS)

Magnesium and Al isotopes were measured in-situ using the Cameca IMS 1280-HR ion microprobe at the SwissSIMS laboratory, University of Lausanne, following in parts a previously described method (Villeneuve et al., 2009). Meteorite chips and San Carlos olivine were mounted together in the inner 15 mm of 1-inch epoxy mounts. Some of the mounts were thinner than 3 mm to reduce sample degassing and improve vacuum conditions. The samples were sputtered with a ~28-30 nA primary O^- static Gaussian beam, operating at 13 kV and focused to ~30-35 μm spot sizes, resulting in typical $^{24}Mg^+$ count rates in olivine and low-Ca pyroxene of >1.4 x 10^9 and >1.0 x 10^9 cps, respectively. Count rates in mesostasis were highly variable, with a few measurements being done with signal intensity as low as ~9 x 10^6 cps for mesostasis with the highest ^{27}Al/^{24}Mg ratios of 69 (MET96503_Ch4) Typical count rates in mesostasis were between 10^7 and 10^8 cps. Secondary ions were accelerated at 10 kV. The Mg and Al ions were measured in multicollection mode using four Faraday cups on the trolleys L'2, C, H1 and H'2. The cups are connected to 10^{10} Ω (^{24}Mg) and 10^{11} Ω (^{25}Mg, ^{26}Mg, ^{27}Al) resistors. The mass resolution of ~2500 (M/ΔM) provided flat peaks at a high ion transfer rate, while the sample chamber and coupling column vacuum was kept between 10^{-9} and 10^{-10} Torr. At this mass resolution $^{24}MgH^+$ is not totally resolved from ^{25}Mg. With the vacuum between 10^{-9} and 10^{-10} Torr the contribution of $^{24}MgH^+$ on ^{25}Mg is negligible (Luu et al., 2013; Liu et al., 2018). Additionally, standards and samples were measured under the same conditions, thus any minor interference from $^{24}MgH^+$ affects both measurements and is eliminated with the IMF correction, which is based on measurements of the reference material.

A typical analysis consisted of 250s presputtering followed by 30 cycles with an integration time of 10s for each isotope. The secondary beam was automatically centered in the transfer and field apertures (DTFAxy and DTCAxy) between presputtering and signal counting, as was the secondary high voltage automatically readjusted by a few V (typically <7 V) to compensate for sample charging if necessary. The background was measured separately for 50s before and after each sample measurement with no primary beam on the sample. Repeated measurements of San Carlos olivine were bracketing each block of unknowns that typically contained 5 to 10 measurements.

The relative sensitivity factors (RSFs), used to correct the relative ion yields of ^{27}Al and ^{24}Mg for different phases {$RSF_{Al/Mg}$ = $(^{27}Al/^{24}Mg)_{measured}$ / $(^{27}Al/^{24}Mg)_{true}$} and the instrumental mass fractionation (IMF) for Mg isotopes were determined using a suite of reference materials. These include olivine standards with different compositions (Mg#81, Mg#91, Mg#99), low- and high-Ca pyroxene, basaltic standard glasses (BCR-2G, BHVO-2G) and *in-house* synthetic dacitic glass. Since terrestrial and meteoritic high-temperature rocks, minerals and their melt products were shown to have the same Mg isotopic compositions at relevant levels of precision, this was accepted also to be valid for all reference materials (e.g. Yang et al., 2009; Teng et al., 2010).

The relative sensitivity factors (RSFs) were determined during each analytical session. The RSF for olivine was ascertained for San Carlos (Mg#91) only (RSF ≈ 1.03 ± 0.01 2SD), as the Al content of the two remaining olivine standards was too low to be precisely determined by EPMA. The RSF for all olivine measurements was therefore assumed to be identical with that of San Carlos olivine during a given session. RSFs for glass and pyroxene reference materials were similar with 0.88 ± 0.01, 0.83 ± 0.01, 0.86 ± 0.01 and 0.88 ± 0.01(all 2SD) (during a single session) for low-Ca pyroxene, high-Ca pyroxene, BHVO-2G and BCR-2G, respectively. Even though the selection of glass reference materials does not cover the whole compositional range of meteoritic mesostasis analysed, this has no significant influence on the applied RSF corrections. All glass and pyroxene reference materials have nearly identical RSFs which is assumed to also be valid for feldspar-normative glass. This assumption is supported by data presented by Luu et al., (2013) who showed that, using a very similar analytical setup, RFSs were nearly identical among all silicate phases analysed.

The Mg-isotopes define a linear trend in a $\delta^{25}Mg'$ vs. $\delta^{26}Mg'$ diagram for SIMS analysis of different reference materials, with $\delta^{i}Mg' = 1000 \times ln\{(\delta^{i}Mg + 1000)/1000\}$ and *i*=25 or 26 (Fig. 2a). This IMF trend is used to correct for isotope fractionation during analysis of natural samples. During some SIMS sessions the fractionation for olivine was slightly different from that for pyroxene and glass. For these measurements the corresponding fractionation laws were applied. IMF and RSFs were determined at the beginning of each session and were recalibrated every 1 to 3 days, depending on machine stability.

The δ^{26}Mg* was calculated as follows: Raw δ^{i}Mg values were converted to δ^{i}Mg' values. Then δ^{26}Mg*' was calculated as the deviation from the IMF law using

$$\delta^{26}Mg^{*\prime} = \delta^{26}Mg' - \{(1/\beta) \times \delta^{25}Mg' - (1/\beta) \times b\}$$

with β the exponential factor and b the intercept from the mass fractionation law. The fractionation-corrected ^{26}Mg/^{24}Mg isotope ratios were calculated using

$$(^{26}Mg/^{24}Mg)^{sample}_{fract.-corrected} = exp(\,\delta^{26}Mg^{*\prime}/1000) \times (^{26}Mg/^{24}Mg)_{standard}.$$

Finally, the excess δ^{26}Mg due to in-situ decay of ^{26}Al was calculated according to

$\delta^{26}Mg^{*} = [\{(^{26}Mg/^{24}Mg)_{sample\ frac.-corrected}/(^{26}Mg/^{24}Mg)_{standard}\}-1] \times 1000$.

This approach is similar to that described by Luu et al. (2013), if a) variation in δ^{25}Mg are due to instrumental fractionation only or b) SIMS and natural fractionation laws are similar and ^{27}Al/^{24}Mg ratios are moderate. Uncertainties on the final δ^{26}Mg* were calculated by error propagation taking into account the internal (counting) errors on the ^{25}Mg/^{24}Mg and ^{26}Mg/^{24}Mg isotopic ratios (typically between 0.02 and 0.06‰ 2s.e. for δ^{25}Mg on reference materials and most meteoritic samples, but could be as large as 0.3‰ in rare cases) as well as the external reproducibility (2SD) on the δ^{26}Mg* mean calculated for all reference materials during a given session. A 2σ filter was applied to the δ^{26}Mg*-values calculated for the 30 cycles of a single measurement and individual cycles outside 2σ were deleted. No more than three cycles were deleted for a given analysis to keep close to the 95% confidence level. Figure 2b shows the fractionation-corrected δ^{26}Mg* for 25 measurements on 7 different reference materials that yield $(\delta^{26}Mg^{*})_{avg.}$ = 0.00 ± 0.06‰ (2σ) (2s.e. = ±0.01‰), attesting to the validity of the applied fractionation correction.

$(^{26}Al/^{27}Al)_0$ and initial ^{26}Mg/^{24}Mg $\{(^{26}Mg/^{24}Mg)_0\}$ were calculated from isochrons regressions fitted using the Model 1 fit of the Isoplot software (Ludwig 2003). The ^{26}Al-^{26}Mg ages of chondrules from this study, and of chondrule data taken from the literature, are calculated relative to CAI (Δt_{CAI}) using the canonical $^{26}Al/^{27}Al = 5.23 \times 10^{-5}$ with the $^{26}Al_{t1/2}$ half-life of 7.17×10^{5} a and assuming homogeneity of ^{26}Al in the early solar system (see *5.1*). All uncertainties are reported as 2 standard deviations, or 95% confidence limit for some ages (Table 1).

2.1.1 Natural mass fractionation (correction) and SIMS

Magnesium isotope ratios of meteorites measured by SIMS can vary due to (i) intrinsic (natural) mass fractionation imparted during chondrule formation and chondrule re-processing and (ii) laboratory induced fractionation during the SIMS analysis. Intrinsic fractionation due to evaporation and condensation processes can be described by the "exponential law" with β = 0.511; though alternative fractionation laws with coefficients mostly between 0.511 and 0.514 were proposed (Davis et al., 2015, and references therein). SIMS Mg isotope fractionation is typically of the form $\delta^{25}Mg' = \delta^{26}Mg' \times \beta + b$ and contains a mass-independent component if $\beta \neq 0$. Theoretically, two separate fractionation corrections for machine and intrinsic mass fractionation would be most appropriate as discussed by Luu et al. (2013) and were likely applied to data by Villeneuve et al. (2009) (their supporting online material). However, both studies do not give enough details how the appropriate SIMS fractionation coefficient ($\alpha^{25}Mg$) for a given measurement was derived. To a first order, fractionation of Mg isotopes during SIMS analysis correlates with Mg content (Fig. 2a). Instrumental mass fractionation occurring during SIMS analyses cannot be corrected for by deducing fractionation factors from the three-isotope diagram. In order to correct meteoritic samples that contain radiogenic ^{26}Mg, fractionation must be first determined and corrected using $\delta^{25}Mg$. A universal law that describes the instrumental fractionation during SIMS analyses for the correction of $\delta^{25}Mg$ precisely and accurately for olivine, pyroxene and glass samples has not been found during the course of this study. This made a separate SIMS fractionation correction, especially for chemically diverse mesostasis in chondrules, impossible. Furthermore, SIMS fractionation for the same reference material can vary by up to 1‰/amu during a single session, although constant analysis conditions reduce these variations to $\alpha^{25}Mg \ll 1$‰/amu (Fig. 2a). Yet, fractionation variations within the same reference material stem from analytical parameters and made it impossible to precisely derive SIMS fractionation coefficients from Mg content, bulk chemistry or generally sample matrix alone. A correlation for fractionation in $\delta^{25}Mg$ as a function of chemical composition and analytical parameters that could be read out from each measurement is therefore key for a separate SIMS fractionation correction that would allow to resolve natural Mg isotope fractionation at levels <1‰, but was beyond the scope of this study.

Since matrix effects on instrumental mass fractionation were not fully quantifiable during this study, a two-step correction would have introduced additional uncertainties. Therefore, a single step correction as described above was applied to OC samples for which intrinsic mass fractionation is reported to be negligible. This correction is inappropriate when strongly fractionated samples like CAIs are analysed and might be problematic for some CCs for which intrinsic Mg isotope fractionation has been reported recently (Ushikubo et al. (2013). However, as long as SIMS and intrinsic Mg isotope fractionation are similar (the mass-independent component of SIMS IMF must be kept small), natural Mg isotope fractionation will be corrected properly by applying a single-step approach.

2.1.2 Dendrites in mesostasis and sample surface quality

Due to the spot size applied in this study some measurements in mesostasis integrate "pure" glass and submicron to micron-sized Ca-pyroxene dendrites. Recently, Nagashima et al. (2017) discussed that such analyses might result in mixing lines rather than isochrons and argued that ^{27}Al/^{24}Mg ratios cannot be properly corrected for relative ion yields. The latter can be problematic if RSFs for pyroxene differ from that of glass and/or plagioclase which has been reported by Nagashima et al (2017) using an EM setup. However, using the approach described above, the correction for relative ion yields does not bias mixed phase measurements, since the RSFs for pyroxene and glass are very similar (see *2.1*). The small difference in RSFs between pyroxene and glass that could impact on the ion yield corrected ^{27}Al/^{24}Mg of mixed-phase measurements in mesostasis is accounted for in the assigned ±8% uncertainty. As discussed before, Mg isotope fractionation in SIMS follows a common IMF law for all reference materials (Fig. 2a) and even during the sessions where SIMS fractionation for olivine differed from pyroxene and glass, the latter always described and were corrected using a common fractionation law. Given that dendrites are small (<few μm) and make only a few % of the total area analysed, mesostasis measurements are therefore not systematically biased by analytical issues or during data correction. The (small scale) mixing of radiogenic (Al-rich glass) and unradiogenic (Mg-rich dendrites) material during the analysis will always be along the tie-line that corresponds to the isochron of a single chondrule. Accepting that chondrules remained closed-systems after crystallisation such measurements can be used to construct internally consistent isochrons.

Yet, if the dendrites are large (≥several μm wide) and their relative abundance is high, small effects on the sputtering-induced fractionation cannot be ruled out and such data must be carefully evaluated for anomalous results indicated by poor correlation of ^{26}Mg excess with ^{27}Al/^{24}Mg. Some chondrules (e.g. MET96503_Ch2, MET96503_Ch11, MET00526_Ch1) contain large amounts of pyroxene dendrites homogeneously distributed in the mesostasis and no spots in these samples were measured in "pure" glass. These chondrules yield (^{26}Al/^{27}Al)$_0$ of (8.0 ± 2.4) × 10^{-6}, (3.7 ± 3.6) × 10^{-6} and (6.0 ± 2.6) × 10^{-6} which have tendencially larger uncertainties, but fall in the range described by chondrules that have no dendrites in the mesostasis. In some chondrules only single measurements were obtained from dendrite-rich mesostasis and anomalous offsets from the isochron regressions for these measurements were not observed.

There are potential analytical error sources that can have significant effects on the resulting ages, one of which is the SIMS sensitivity to the quality of the sample surface. Especially small cracks present before the measurement or developing during the analysis can strongly impact on the sputtering behaviour, such that the fractionation effects will differ from that of the reference materials. This can lead to erroneous results, if all analyses for a given chondrule are automatically used for the isochron regression without a careful evaluation of the single measurements. As such spots are not always recognized by their internal uncertainties, they need to be identified by SE and BSE imaging before and after SIMS analysis and excluded from the isochron dataset. Figure 3 shows an extreme example for the impact of an inappropriate sample surface (cracks) on the SIMS fractionation and the resulting isochron diagram.

2.2 Electron microprobe analysis (EMPA)

All analyzed chondrules were studied before and after SIMS analysis by reflected light microscopy and secondary electron (SE) and backscattered electron (BSE) imaging. Mineral compositions and "bulk chondrule" $^{27}Al/^{24}Mg$ ratios were determined by spot measurements and standardized elemental mapping (Lanari et al., 2014) using a microprobe JEOL JXA-8200 Superprobe at the University of Bern. Acceleration voltage and beam current were set at 15 kV (all measurements) and 15-20 nA or 80-120 nA for point measurements and mapping, respectively, with spot sizes between 1 μm (minerals and maps) and 5-7 μm (mesostasis). Element concentrations were measured using five wavelength-dispersive spectrometers (WDS). Automated matrix correction was done with the CITZAF package (Armstrong, 1995).

3. Samples

This study presents Mg isotope data for 31 chondrules from seven UOCs: MET 00452, MET 96503, QUE 97008, MET 00526, NWA 8276, NWA 5206 and NWA 7936 which cover L, LL and intermediate L(LL) chondrites of petrologic grades from 3.00 to 3.15. The classifications used here have been adopted from the Meteoritical Bulletin Database, 2018. The low petrologic types for some of the samples (QUE 97008, MET 00526 and MET 96503) have been studied in detail in the original Cr study by Grossman and Brearley (2005). The focus on low petrologic type avoids the risk of Mg isotope disturbance due to high-temperature metamorphism and alteration on the chondrite parent body (e.g. Kita et al., 2000). The analysed chondrules are all ferromagnesian and have porphyritic olivine (PO), porphyritic olivine-pyroxene (POP) and porphyritic pyroxene (PP) textures, mostly of Fe-rich type II. Two analysed chondrules are magnesian type I.

SIMS measurements were limited to chondrules that reveal several and large areas (>30-40 μm) of mesostasis which is the material in chondrules with highest $^{27}Al/^{24}Mg$ and thus key to obtain reliable and precise age information for individual chondrules. Mesostasis areas in the majority of chondrules are typically smaller. The analysed chondrules typically have diameters <1 mm, with very few exceptions up to 2.4 mm, and therefore sample the major chondrule size distribution of ordinary chondrites. A total of 4 to 17 SIMS spots in crystals and mesostasis were measured in one single chondrule.

Four chondrules from QUE 97008 have been studied before for Al-Mg systematics (Rudraswami and Goswami, 2007) and gave $(^{26}Al/^{27}Al)_0$ between $(1.95 \pm 0.76) \times 10^{-5}$ and $(7.9 \pm 3.6) \times 10^{-6}$. No ^{26}Al-^{26}Mg or Pb-Pb chondrule ages have been published yet for the remaining samples selected for this study. Sample NWA 8276 has been classified as L3.00 based on Cr systematics in ferroan olivine and is a rare meteorite with only one additional sample having the same classification (NWA 7731, likely pairing with NWA 8276; Meteoritical Bulletin Database, April 2018).

Most studied chondrules appear round to oval in the polished section and likely sample cuts of whole chondrules. Some analysed chondrules from the edge of the section are only fragments of previously larger chondrules. Relict grains that might indicate reworking of chondrules or mixing with pre-existing chondrules are rare in the studied samples. Only the type-II PO chondrule MET96503_Ch3 contains a single olivine core with Fo97 whereas the remaining Ol phenocrysts have Fo87. The two analysed POP type-I chondrules show a weak (NWA8276_Ch2) to strong (MET00452_Ch22) mineralogical zonation where olivine occurs preferentially in the centre of the chondrules.

The sample names and chondrule types are listed together with the isotope data in Table 1. A brief petrographic description for each of the analysed chondrules, including any special characteristics, and representative BSE images of the studied chondrules can be found in the online Supplement (Fig. S1, S2).

4. Results

All analysed chondrules have ferromagnesian compositions with bulk Al_2O_3 contents <10 wt% and typical bulk $^{27}Al/^{24}Mg$ ratios of 0.06 - 0.27. Maximum $^{27}Al/^{24}Mg$ ratios in mesostasis do not correlate with $(^{26}Al/^{27}Al)_0$ which would be indicative for a systematic analytical bias caused by improper fractionation correction. Excess ^{26}Mg was recorded in all but one magnesian type I POP chondrule (NWA 8276_Ch2) (Fig. 1b). Calculated (^{26}Al/^{27}Al)$_0$ for all chondrules range from (9.5 ± 2.8) × 10^{-6} to (3.1 ± 1.2) × 10^{-6} which translates into relative ages (Δt_{CAI}) between $1.76^{+0.36}_{-0.27}$ and $2.92^{+0.51}_{-0.34}$ Ma (Fig. 4). No chondrule was found to have (^{26}Al/^{27}Al)$_0$>10^{-5}. Typical uncertainties for the age estimates for single chondrules are between ±0.15 and ±0.5 Ma (2σ).

L-chondrites

Three chondrules in **QUE 97008 (L3.05)** record (^{26}Al/^{27}Al)$_0$ of (8.8 ± 1.3) × 10^{-6} - (5.6 ± 1.6) × 10^{-6} with δ^{26}Mg*$_0$ between -0.012 ± 0.070‰ and 0.019 ± 0.059‰ resulting in Δt_{CAI} of $2.31^{+0.35}_{-0.26}$, $1.84^{+0.16}_{-0.14}$ and $2.16^{+0.29}_{-0.23}$ Ma. ^{27}Al/^{24}Mg ratios in the mesostasis of an individual chondrule can show a narrow spread like in Ch8 and Ch13, where they range from 6-7 and from 7-10, respectively. This relative homogeneity contrasts with Ch9 that shows a range in ^{27}Al/^{24}Mg from 7 to 21. Chondrules from the same sample analysed before (Rudraswami and Goswami, 2007) gave higher (^{26}Al/^{27}Al)$_0$ between (7.9 ± 3.6) × 10^{-6} and (1.95 ± 0.76) × 10^{-5}.

Four chondrules in **NWA 8276 (L3.00)** show resolvable excess ^{26}Mg and yield (^{26}Al/^{27}Al)$_0$ between (9.5 ± 2.8) × 10^{-6} and (4.3 ± 1.6) × 10^{-6} and δ^{26}Mg*$_0$ between -0.020 ± 0.028‰ and 0.002 ± 0.027‰ that correspond to ages of $2.11^{+0.24}_{-0.19}$, $2.58^{+0.48}_{-0.33}$, $1.76^{+0.36}_{-0.27}$ and $2.27^{+0.26}_{-0.21}$ Ma. Three chondrules have ^{27}Al/^{24}Mg ratios <7 and one chondrule records ^{27}Al/^{24}Mg ratios in mesostasis between 2 and 31. NWA 8276 Ch2 (Fig. 1b) does not record excess ^{26}Mg and defines a negative (^{26}Al/^{27}Al)$_0$ = (-1.2 ± 3.8) × 10^{-6} with the intercept δ^{26}Mg*$_0$ = 0.007 ± 0.072‰, both at 95% confidence level with low ^{27}Al/^{24}Mg of 3-4 in the mesostasis.

Nine chondrules from **MET 96503 (L3.1)** record (^{26}Al/^{27}Al)$_0$ between (9.4 ± 1.5) × 10^{-6} and (3.1 ± 1.2) × 10^{-6} with δ^{26}Mg*$_0$ between -0.019 ± 0.058‰ and 0.008 ± 0.040‰, resulting in Δt_{CAI} of $1.94^{+0.37}_{-0.27}$, $2.58^{+0.79}_{-0.44}$, $2.33^{+0.19}_{-0.16}$, $1.78^{+0.18}_{-0.15}$, $1.86^{+0.20}_{-0.16}$, $2.21^{+0.35}_{-0.26}$, $2.41^{+0.62}_{-0.39}$, $2.74^{+}_{-0.70}$ and $2.92^{+0.51}_{-0.34}$ Ma. Five chondrules record ^{27}Al/^{24}Mg <7 and Ch4 (Fig. 1a) has a ^{27}Al/^{24}Mg of 69 which is the highest value in all chondrules.

One chondrule (Ch2) from **NWA 7936 (L3.15)** records (^{26}Al/^{27}Al)$_0$ of (4.8 ± 1.2) × 10^{-6} with δ^{26}Mg*$_0$ of 0.002 ± 0.033‰ and the resulting age (Δt_{CAI}) of $2.47^{+0.30}_{-0.23}$ Ma. ^{27}Al/^{24}Mg ranges from 10-14.

L(LL)-chondrites

Four chondrules in **MET 00526 (L(LL)3.05)** give (^{26}Al/^{27}Al)$_0$ between (7.8 ± 1.4) × 10^{-6} and (5.5 ± 1.7) × 10^{-6} and δ^{26}Mg*$_0$ between -0.002 ± 0.044‰ and 0.011 ± 0.037‰ corresponding to Δt_{CAI} of $2.24^{+0.59}_{-0.37}$, $1.97^{+0.20}_{-0.17}$, $2.33^{+0.38}_{-0.28}$ and $2.04^{+0.14}_{-0.12}$ Ma. ^{27}Al/^{24}Mg ratios in Ch1 and Ch8 are relatively low and homogeneous with ~2.5 and ~5, respectively. Samples Ch7 and Ch10 show larger variability in Al/Mg with ranges from 3-12 and 6-24, respectively.

Four chondrules from **MET 00452 (L(LL)3.05)** have $(^{26}Al/^{27}Al)_0$ between (7.34 ± 0.99) × 10^{-6} and (3.1 ± 1.6) × 10^{-6} and $\delta^{26}Mg^*_0$ between -0.017 ± 0.038‰ and 0.011 ± 0.039‰. ^{26}Al-^{26}Mg ages (Δt_{CAI}) are $2.76^{+0.50}_{-0.34}$, $2.03^{+0.15}_{-0.13}$, $2.92^{+0.75}_{-0.43}$ and $2.43^{+0.34}_{-0.26}$ Ma. $^{27}Al/^{24}Mg$ ratios in mesostasis are variable with 6-7 (Ch14), 4-27 (Ch21) and 5-16 (Ch23). Ch22 (Fig. 1d) shows relatively low and homogeneous $^{27}Al/^{24}Mg$ ratios of 4-7 in the mesostasis.

LL-chondrite

Five chondrules from **NWA 5206 (LL3.05)** yield $(^{26}Al/^{27}Al)_0$ between (7.76 ± 0.82) × 10^{-6} and (4.07 ± 0.97) × 10^{-6} and $\delta^{26}Mg^*_0$ between -0.019 ± 0.067‰ and 0.008 ± 0.023‰ with resulting ^{26}Al-^{26}Mg ages Δt_{CAI} of $2.26^{+0.70}_{-0.41}$, $2.35^{+0.28}_{-0.22}$, $1.97^{+0.12}_{-0.10}$, $2.51^{+0.25}_{-0.20}$ and $2.64^{+0.28}_{-0.22}$ Ma for Ch1, Ch7, Ch8, Ch10 and Ch11, respectively.

Of all analysed chondrites MET 96503 (L3.1) shows the largest spread in $(^{26}Al/^{27}Al)_0$ ranging from (9.4 ± 1.5) × 10^{-6} to (3.1 ± 1.2) × 10^{-6}. In this sample also the highest number of chondrules (9) could be analysed. NWA 8276, which is the sample of lowest petrologic type (L3.00), yields the slightly oldest chondrule age ($1.76^{+0.36}_{-0.27}$) while the other chondrules from this sample agree well with the general age range of OC chondrules. Only one chondrule could be analysed in sample NWA 7936, which is the meteorite of the highest petrologic type (3.15) selected for this study. It yields an age that agrees with the range defined by chondrules from the other meteorite samples.

The range of $(^{26}Al/^{27}Al)_0$ in chondrules from single samples is similar between the different chondrites analysed. Systematic trends in $(^{26}Al/^{27}Al)_0$ or in mesostasis Mg isotopic systematic (e.g. data scatter/goodness of fit of the isochron) correlating with the petrologic type are not observed. Uncertainties on the isochron regression broadly correlate with maximum measured $^{27}Al/^{24}Mg$ in the mesostasis which indicates that most isochrons are unaffected by systematic analytical errors or scattering of the data points due to disturbance of the Mg isotope system. This correlation is most significant for samples with $^{27}Al/^{24}Mg$ <5, which mostly applies to chondrules that contain high amounts of pyroxene dendrites. For these samples the uncertainties on the correlated ^{26}Al-^{26}Mg ages are consequently larger. Four isochrons (MET965203_Ch8, MET96503_Ch17, NWA8276_Ch1, MET00452_Ch23) have MSWD>2.5 and thus scattering of data for these chondrules is slightly larger than analytical uncertainty (Fig. 5). The low MSWDs for most of the remaining isochron regressions substantiate the unaltered character for the majority of investigated samples and supports the hypothesis, that Mg isotopes remained unaffected by thermal metamorphism.

The initial $^{26}Mg/^{24}Mg$ ratios ($\delta^{26}Mg^*_0$) of the analysed chondrules are identical within uncertainties and range from -0.020 ± 0.028‰ to 0.011 ± 0.039‰. The ingrowth of radiogenic ^{26}Mg in a chondritic uniform reservoir (CHUR) between 1.5 and 3.0 Ma of 7 ppm, calculated for a chondritic $^{27}Al/^{24}Mg$ of 0.101 and the canonical $^{26}Al/^{27}Al$ of 5.23×10^{-5}, cannot be resolved by the SIMS measurements. Even if chondrule precursors separated early from the chondritic reservoir with a fractionated $^{27}Al/^{24}Mg$ of 0.3 (the highest bulk for any of the analysed chondrules) they would have developed not more than ~20 ppm excess ^{26}Mg over the 1.5 Ma time interval of chondrule formation. The measured $\delta^{26}Mg^*_0$ and corresponding uncertainties are mainly controlled by analyses in mafic phases and uncertainties on $\delta^{26}Mg^*_0$ are therefore overestimated by the assigned analytical errors for chondrules in which only few measurements in mafic phases were acquired. All $^{26}Mg/^{24}Mg$ ratios obtained from measurements in mafic phases during the course of this study sample a close to normal distribution. Since all chondrules have analytically indistinguishable initial $^{26}Mg/^{24}Mg$ ratios it is possible to use the combined data from all olivine and pyroxene analyses as the initial $^{26}Mg/^{24}Mg$ ratio for all chondrules. The initial $^{26}Mg/^{24}Mg$ ratios estimated this way have an uncertainty of ±0.0063‰. The resulting isochrons yield similar $(^{26}Al/^{27}Al)_0$ and chondrule model ages compared to the original isochrons but have generally smaller uncertainties (Table1).

Detailed isotopic data for all chondrules are listed in Table 1 and in the Supplement (Table S1). Representative major and minor oxide concentrations in olivine, pyroxene and glass are summarized in Table S2. The isochron diagrams for the individual measurements of minerals and mesostasis for single chondrules are shown in Fig. 5.

5. Discussion

5.1 Distribution of ^{26}Al in the early solar system

The interpretation of the $^{26}Al/^{26}Mg$ systematics of meteorites and their components as a chronometer relies on the assumption that the $(^{26}Al/^{27}Al)_{initial}$ ratio was constant throughout the solar nebular when the different components formed. Regional variation of ^{26}Al in the solar nebular would make a comparison of ages among different meteorite classes tenuous and possibly limit the use of the chronometer for the determination of relative ages within individual classes. Thus, to evaluate the chronological significance of $(^{26}Al/^{27}Al)_0$ obtained from isochron diagrams it is necessary to discuss the distribution of ^{26}Al in the early solar system.

^{26}Al heterogeneity in meteorites has been reported for refractory components like ^{16}O-rich corundum condensates (Makide et al., 2011), spinel-hibonite spherules (SHIBs) (Liu et al., 2012) and FUN (fractionated and unknown nuclear isotope anomalies) CAIs (e.g. Park et al., 2017). The Al isotopic composition in these early condensates can be attributed to isotopic heterogeneity of the molecular cloud from which they formed and that predates the homogenisation of the PPD in which chondrules were formed. They are thus helpful to study the earliest solar system composition but are no suitable tracers of the isotopic composition of the reservoir in which chondrules formed. Recently, Larsen et al. (2011) suggested a large-scale heterogeneity for ^{26}Al of up to 80% of the canonical value throughout the inner solar system after formation of first solids. They presented a combined isochron of CAIs and AOAs from the reduced CV chondrite Efremovka that yields $\delta^{26}Mg^*_0$ = -0.0159 ± 0.0014‰ which is a significantly higher than the expected initial $^{26}Mg/^{24}Mg$ of -0.038‰ calculated with a canonical $^{26}Al/^{27}Al$ of (5.23 ± 0.13) × 10^{-5} and a Solar $^{27}Al/^{24}Mg$ of 0.101. Wasserburg et al. (2012) showed that, by excluding AOAs and forsterite-rich accretionary rims from the Larsen et al. (2011) regression the isochron would yield an initial $^{26}Al/^{27}Al$ = (5.32 ± 0.18) × 10^{-5} and $\delta^{26}Mg^*_0$ = -0.030 ± 0.040‰, both in agreement with the canonical CAIs from CV Allende (Jacobsen et al., 2008). The main arguments for a disc-wide Al isotopic heterogeneity by Larsen et al. (2011) were based on model isochrons for various inner solar system materials that were constructed with the assumption that the solar system initial Mg isotopic composition was homogeneous at the level of ±1.4 ppm (deduced from their AOA-CAI isochron) and that Al/Mg fractionation of the samples from the chondritic value occurred after decay of ^{26}Al. The validity of these assumptions was questioned by later studies (e.g. Wasserburg et al., 2012, Kita et al., 2013). MacPherson et al. (2017) showed that $(^{26}Al/^{27}Al)_0$ values of at least some CV FoBs and AOAs are consistent with the canonical value which might justify their use to more precisely constrain the initial Mg isotopic composition of refractory condensates. In any case, additional studies are needed to better evaluate the initial Mg isotopic composition of different early solar system materials.

Many published chondrule Pb-Pb ages, most acquired from aliquots of pooled chondrules, agree well with ^{26}Al-^{26}Mg chondrule ages (e.g. Amelin et al., 2002; Amelin and Krot, 2007; Connelly and Bizzarro, 2009). Two recent studies (Connelly et al., 2012; Bollard et al., 2017) report Pb-Pb ages from stepwise leaching of single chondrules of which 14 fall within the ~1.8 Myr *time gap* between CAIs and the majority of ^{26}Al-^{26}Mg chondrule ages. Some chondrules from these studies yield Pb-Pb ages as old as CAIs. These old Pb-Pb ages question the canonical ^{26}Al abundance for the OC and CC reservoirs and suggest a heterogeneous distribution of this short-lived isotope during the time chondrules formed. Because of the relatively high amount of sample material needed, most single chondrule Pb-Pb ages were acquired from exceptionally large chondrules (~6 to 16 times larger than L-chondrite chondrule mean size (Weisberg et al., 2006; Metzler 2018)), many of which have non-porphyritic barred or skeletal textures. Both, the unusual large chondrule size and the mostly non-porphyritic textures are different compared to chondrules for which ^{26}Al-^{26}Mg ages are reported. Previously, it has been suggested that the Pb-Pb system could be affected by later isotopic disturbance on the parent body (Kita et al., 2015). Another aspect regarding the chronological meaning of Pb-Pb dates that might need consideration is the loss of ^{222}Rn (half-life $t_{1/2}$ = 3.8 d) in the ^{238}U-^{206}Pb decay chain from chondrules. Radon escape from terrestrial rocks and minerals (e.g. Eakin et al., 2016) occurs in diverse geological settings where ^{222}Rn undergoes recoil from ^{226}Ra decay and the escape to production ratios in accessory minerals and (ultra)mafic rocks can reach several percent. Radon mobility is often higher than predicted from its low diffusivity since radiation damage of the host phase, caused by alpha decay and nuclear fission, provides pathways for enhanced Rn migration (e.g. Rama and Moore, 1984; Eakin et al., 2016), which can result in significant ^{222}Rn mobilisation in soils and crystalline rocks. The activity ratio of ^{238}U (half live $t_{1/2}$ = 4.5 Ga) and ^{234}U (half-life $t_{1/2}$ = 0.25 Ma) in the interstellar medium and the protoplanetary disk is close to unity and thus the ^{222}Rn activity in a chondrule is highest at or shortly after its formation. As most of the radiogenic Pb component in chondrules is associated with the mesostasis (Bollard et al., 2017), it also contains the majority of U and, consequently, is the production site of radiogenic Rn. At the same time, the mesostasis is also enriched in Al and silicic glass is highly vulnerable to radiation damage by high-energetic gamma rays. ^{222}Rn emanation from the chondrule could thus be enhanced shortly after the chondrule formed due to radiation damage of the mesostasis by high ^{26}Al activity. This effect will be less critical for chondrules that formed after most ^{26}Al had decayed but could enhance early ^{222}Rn loss from chondrules. Assuming ^{222}Rn emanation from a chondrule for a duration of 1.5 Myr after formation would cause a 0.5‰ loss of the total radiogenic ^{206}Pb that accumulated over the life-time of the chondrule. In principle less than 0.8‰ of radiogenic ^{206}Pb loss due to ^{222}Rn escape from a chondrule would change the ^{204}Pb/^{206}Pb and ^{207}Pb/^{206}Pb ratios such that the corresponding ^{207}Pb-^{206}Pb ages would shift by more than 1 Myr - towards older dates. Even though terrestrial rocks and minerals are unlikely best analogues for potential ^{222}Rn escape in meteorites, the first measurements of ^{222}Rn loss from bulk meteorites demonstrate that ^{222}Rn emanation can be significant (Girault et al., 2017). So far, the old Pb-Pb ages for chondrules are unique to the Pb-Pb chronometer and have not been found for chondrules that have been dated with short-lived chronometers including ^{26}Al-^{26}Mg. Considering the conclusions drawn for Al inhomogeneity, further studies should be conducted to exclude this potential error source.

In contrast, homogeneity of ^{26}Al and the chronological significance of ^{26}Al-^{26}Mg have been suggested by numerous studies (e.g. Villeneuve et al., 2009; Kita et al., 2013; Mishra and Chaussidon, 2014), encompassing diverse methodical approaches and a wide variety of meteorite components. The cross-correlation of a CV CAI Pb-Pb age with the ^{26}Al-^{26}Mg model age for the same sample by Bouvier & Wadhwa (2010) shows good agreement between the two chronometers and argues for ^{26}Al homogeneity and a canonical ^{26}Al abundance in the young solar nebular. Comparison of Hf-W and Al-Mg relative ages for angrites D'Orbigny and Sahara 99555 does not indicate large-scale ^{26}Al heterogeneity for the CAI and angrites forming reservoirs (Kruijer et al., 2014). Furthermore, the concordance of $(^{26}Al/^{27}Al)_0$ and ^{182}Hf/^{180}Hf for four different meteorite samples (bulk CAIs, angrites and CR and CV chondrules from the Kaba meteorite) agrees with the expected slope from ^{26}Al and ^{182}Hf decay constants and argues for homogeneous distribution of ^{26}Al at a level of better than ±10% after 1.6 Ma and a closed-system evolution of a ^{26}Al/^{27}Al reservoir defined by CAIs from CV meteorites (Budde et al. 2018, and references therein). Although no OC samples were considered in the latter study, the selected samples, which formed in different reservoirs and during different times in the PPD, give strong evidence that the reported homogeneity reflects the whole PPD in space and time. It should be noted, that the ^{182}Hf-^{182}W ages for chondrules from CV meteorites were obtained from a batch of hundreds of chondrules and therefore reflect chondrule mean ages that do not inevitably exclude the presence of single old chondrules (Budde et al., 2016b).

Magnesium isotope analysis of bulk chondrules from the Allende meteorite yield initial ^{26}Al/^{27}Al between $(1.84 \pm 0.80) \times 10^{-5}$ and $(6.41 \pm 1.23) \times 10^{-5}$ (Bizzarro et al., 2004) (Fig. 4), the latter being identical within error to the canonical value of $(5.23 \pm 0.13) \times 10^{-5}$. As pointed out by the authors, a wide spread mixing of CAI and chondrule-like material in those samples is unlikely. The high $(^{26}Al/^{27}Al)_0$ is therefore difficult to reconcile with a scenario that involves reduced inner solar system ^{26}Al/^{27}Al, as it would require later removal of Al or addition of isotopically heavy Mg, both being unlikely scenarios. The more straightforward explanation is that these samples reflect the Al isotopic composition of the chondrule precursor material at the time of chemical fractionation from the chondritic reservoir (Bizzarro et al., 2004; Luu et al., 2015) and yield additional strong evidence for a non-reduced but canonical Al isotopic composition at least for the CC chondrule forming reservoir.

There is no consensus whether or not ^{26}Al was homogeneously distributed in the PPD in space and time relevant for the interval of chondrule formation. As a consequence, ^{26}Al-^{26}Mg mineral isochron ages can be interpreted to either reflect a date with absolute age significance if ^{26}Al was homogeneously distributed throughout the inner solar system and the canonical value is universally valid, or, in case of ^{26}Al heterogeneity, the initial ^{26}Al/^{27}Al of chondrules reflect the Al isotopic composition of a certain place in the disc. In this case the calculated absolute age may be biased yet the relative ages between chondrules would still be correct. The Mg isotope data obtained in this study are discussed in a chronological context under the assumption of ^{26}Al homogeneity throughout the innermost PPD. Even in the scenario of a homogeneous but reduced ^{26}Al abundance in the chondrule forming reservoirs, the ^{26}Al-^{26}Mg system yields significant relative age information on chondrule formation with the highest age resolution of all chronometers.

5.2 Initial ^{26}Al/^{27}Al and corresponding ^{26}Al-^{26}Mg ages

This study comprises the largest number of OC chondrules, all of low petrologic type, for which Al-Mg isotopes were measured during the course of a single study. The total range of initial ^{26}Al/^{27}Al recorded by chondrules from this study is (9.5 ± 2.8) × 10^{-6} - (3.1 ± 1.2) × 10^{-6} which translates into relative ages (Δt_{CAI}) of $1.76^{+0.36}_{-0.27}$ to $2.92^{+0.51}_{-0.34}$ Ma (Fig 6a). Generally, neither (^{26}Al/^{27}Al)$_0$ distribution nor the uncertainties on single chondrule dates indicate a trend with petrologic type (Fig. 6). This confirms that (^{26}Al/^{27}Al)$_0$ and the corresponding chondrule ages are undisturbed by metamorphic overprint on the chondrite parent body.

While the general range reported here is similar to previously published (^{26}Al/^{27}Al)$_0$ for ferromagnesian chondrules (Villeneuve et al., 2009, Kita and Ushikubo, 2012), it differs insofar as no single chondrule was found that records (^{26}Al/^{27}Al)$_0$>10^{-5}. Figure 6b shows that neither L- or LL-chondrites nor single meteorite samples contain chondrules with unique (^{26}Al/^{27}Al)$_0$ distributions that would define a single age or a distinct age range. Also, no obvious relation between metamorphic grade and age distribution is visible. Initial ^{26}Al/^{27}Al in L-chondrites range from (9.5 ± 2.8) × 10^{-6} to (3.1 ± 1.2) × 10^{-6} with resultant ages between $1.76^{+0.36}_{-0.27}$ and $2.92^{+0.51}_{-0.34}$ Ma, which is similar to L(LL)- {(7.8 ± 1.4) × 10^{-6} to (3.1 ± 1.6) × 10^{-6} and $1.97^{+0.20}_{-0.17}$ - $2.92^{+0.75}_{-0.43}$ Ma} and LL-chondrites {(7.76 ± 0.82) × 10^{-6} to (4.07 ± 0.97) × 10^{-6} and $1.97^{+0.12}_{-0.10}$ - $2.64^{+0.28}_{-0.22}$ Ma}. Apparently, chondrules from different chondrite groups that are distinct from one another, e.g. having different chondrule size and bulk composition, show no systematic differences in their initial $^{26}Al/^{27}Al$. This implies in turn that, if the group-specific characteristics reflect distinct formation reservoirs, chondrule formation occurred almost contemporaneously or at least during the same time period in distinct regions of the OC reservoir from 1.8 to 3.0 Ma after formation of CAIs. The spread in the analytically different ages for individual chondrules within the same sample and between samples implies either continuous or episodic chondrule formation over a time interval of ca. 1.2 Ma. The isochrons are based on the analysis of mafic minerals with low $^{27}Al/^{24}Mg$ and mesostasis representing melt compositions with high $^{27}Al/^{24}Mg$. The measured Mg-isotope composition of pyroxene and olivine is analytically indistinguishable and uniform. Thus, the isochrons are essentially defined by the analyses of the residual melt component. From this follows that the ages define the time of melt formation. The spread in the ages for the different chondrules implies that melt formed more than once or the chondrules remained partially molten and cooled at somewhat different rates recording their quenching time. Multiple melt formation requires episodic reheating and incomplete remelting of chondrules after their first formation or last complete melting which could cause partial Mg isotopic re-equilibration, and by this would reduce the $^{26}Mg/^{24}Mg$ of the mesostasis. Without complete equilibration, the determined $(^{26}Al/^{27}Al)_0$ does not record equilibration at the time of chondrule formation but indicates a minimum age for the last equilibration or a maximum age for the last heating pulse. Assuming chondrule heating in a closed-system an increase of $(^{26}Al/^{27}Al)_0$ can be excluded. Chondrules with high $(^{26}Al/^{27}Al)_0$ can thus be considered to record the most pristine isotopic compositions preserved from the time of chondrule formation. This argument does not automatically imply partial resetting of chondrules with low initial $^{26}Al/^{27}Al$. In this study, the highest $(^{26}Al/^{27}Al)_0$ of an individual chondrule in the L-chondrites NWA 8276, MET 96503 and QUE 97008 agree within their 1σ uncertainty. Calculating the average age from their weighted mean $(^{26}Al/^{27}Al)_0 = (9.1 \pm 0.9) \times 10^{-6}$ gives $(\Delta t_{CAI})_{mean\ L\text{-}chondrite} = 1.81^{+0.11}_{-0.10}$ Ma. The highest initial $^{26}Al/^{27}Al$ of individual chondrules in six of the seven studied chondrite samples are identical within 2σ uncertainties, yielding the weighted mean $(^{26}Al/^{27}Al)_{0,\ mean} = (8.0 \pm 0.5) \times 10^{-6}$ and a mean age $(\Delta t_{CAI})_{OC\ mean} = 1.81^{+0.07}_{-0.08}$ Ma. The L-chondrite mean age is slightly younger but not resolved from that of the oldest OC chondrules. Accepting these ages to be most robust and likely least disturbed, the mean $(^{26}Al/^{27}Al)_0$ and corresponding average age of the oldest individual chondrules in the L chondrite samples can be interpreted to record a major and punctuated initiation of chondrule formation ~1.8 ± 0.1 Ma after CAI. Since all chondrite samples show a similar spread in chondrule ages they likely formed from a reservoir with homogeneous distribution of ^{26}Al at the time of their formation.

No excess ^{26}Mg from in-situ decay of ^{26}Al was found in the mesostasis of POP chondrule NWA8276_Ch2 (Fig. 1d), one of the two analysed magnesian type-I chondrules, which records an initial bulk Mg isotopic composition of 0.007 ± 0.072‰ poorly defined by the slightly negative regression (Fig. 5). One explanation for this unusual sample is that it formed after ^{26}Al was effectively decayed in the PPD and the chondrule could not evolve sufficient radiogenic ^{26}Mg to be detected by SIMS analysis. This would imply that it formed later than ~3 Ma after CAIs, that is ~1 Myr after the majority of chondrules and probably inconsistent with suggested accretion times of OC parent bodies. Alternatively, the chondrule equilibrated after earlier formation under open system conditions with the chondritic reservoir after ^{26}Al was decayed. Mineralogically and texturally the chondrule does not show obvious signs for a later alteration but shares many similarities with unaltered type-I chondrules from the Semarkona meteorite (Jones and Scott, 1989). The chondrule is mineralogically zoned with olivine preferentially occurring in the inner part of the chondrule. The sub- to euhedral olivine and pyroxene phenocrysts, some of the latter are partly overgrown by thin high-Ca pyroxene rims and poikilitically enclose olivine, have homogeneous major element contents (~Fa4 and Fs2) and are embedded in the mesostasis that lacks pyroxene dendrites and is homogeneously distributed within the chondrule. Either way, this sample may have preserved evidence for late processes that were able to reset or re-equilibrate the Mg isotopic systematic of some chondrules.

5.2.1 Relationship of $(^{26}Al/^{27}Al)_0$ with chondrule type

This study includes analyses from a wide variety of chondrules that differ in texture and composition (see Table 1). Numerous studies addressed a possible genetic relation between ferroan and magnesian chondrules and discussed the formation of type-I chondrules by evaporation and reduction of type-II chondrule material or the opposite scenario in which ferroan chondrules formed by melting and oxidation of magnesian chondrules (e.g. Villeneuve et al., 2015). If a genetic relationship involves a temporal evolution it could be manifested in the initial $^{26}Al/^{27}Al$. As reported by Kita and Ushikubo (2012) ferroan chondrules of CO3.0 meteorite Y-81020 might be slightly younger than magnesian samples, though only few ferroan chondrules were analysed in this sample. Of all ferromagnesian chondrules from OCs for which ^{26}Al-^{26}Mg data are published, type-II chondrules make up the vast majority (>90%), while more than half of analysed CC chondrules belong to type-I. In this study, we analysed two type-I chondrules. The first does not show resolvable excess ^{26}Mg (NWA8276_Ch2) while the second chondrule (MET00452_Ch22) records the lowest initial $^{26}Al/^{27}Al$ of all measured samples with $(3.1 \pm 1.6) \times 10^{-6}$, yielding a late formation age with relatively large uncertainties of $2.92^{+0.75}_{-0.43}$

Ma. Published data of six type-I chondrules include two samples with high $(^{26}Al/^{27}Al)_0$ >10^{-5} while the remaining 4 chondrules have initial $^{26}Al/^{27}Al$ between 7.2 × 10^{-6} and 4.8 × 10^{-6}, similar to type-II chondrules. Initial $^{26}Al/^{27}Al$ of ferroan chondrules show a larger spread, but the number of analysed magnesian samples is about 5 times smaller. Ferroan and magnesian chondrules do not reveal a clear difference in initial $^{26}Al/^{27}Al$. Similar conclusions on a smaller data set of OC chondrules were previously drawn by Kita and Ushikubo (2012). Whether this implies a missing chronological relation or indicates wide-spread partial resetting of chondrules after primary formation is difficult to evaluate as the low number of data, especially for magnesian chondrules, lacks statistical significance.

5.2.2 Age frequency distribution

Previous studies have attempted to identify different generations of chondrules (Villeneuve et al., 2009; Kita and Ushikubo, 2012; Schrader et al., 2017). In Figure 7 the newly acquired data are combined with literature data to construct probability density functions (PDFs) and adaptive Kernel density estimates (KDEs). These can be used to evaluate the possibilities that different ages recorded by different individual chondrules may result from either discrete thermal events or rather reflect a continuum of ages due to a later heating pulse that caused partial resetting or continuous chondrule formation over the time interval recorded by the chondrules. The diagrams include published data for PO, POP and PP ferromagnesian chondrules from OCs (51) and CCs (42) with petrologic types ≤3.15 mostly from the last ~15 years that were obtained by ion probe techniques and for which chondrule types and 2σ errors on the $(^{26}Al/^{27}Al)_0$ were reported (Fig. 7). Aluminum- and plagioclase-rich chondrules (PRCs) for which ^{26}Al-^{26}Mg ages have been published were not included. Even though most of them record initial $^{26}Al/^{27}Al$ similar to ferromagnesian chondrules, it has been shown that PRCs can contain CAI-like material (Kunihiro et al., 2004) and a close genetic relation to CAIs has been reported for Al-rich chondrules (e.g. Krot et al., 2004; Russel et al., 2005, Hutcheon et al., 2000). Consequently, all such samples are excluded from the PDFs because they might contain fossil $^{26}Mg^*$ derived from CAIs, which would bias age information. The vast majority of published OC chondrule data, most of which were acquired from the Semarkona and Bishunpur meteorites, yield initial $^{26}Al/^{27}Al$ between 1.3 × 10^{-5} and 3 × 10^{-6} and out of those, 80% record $(^{26}Al/^{27}Al)_0$< 10^{-5}. Only four chondrules record higher values of up to 2.3 × 10^{-5}. This is a larger spread towards higher $(^{26}Al/^{27}Al)_0$ compared to the data obtained during this study ((9.5 ± 2.8) × 10^{-6} to (3.1 ± 1.2) × 10^{-6}). Notably, one of the four oldest chondrules was reported from QUE 97008 meteorite, yielding an initial $^{26}Al/^{27}Al$ of (1.95 ± 0.76) × 10^{-5} (Rudraswami et al., 2008).

Three chondrules from the same sample were measured also during this study but none was found that recorded $(^{26}Al/^{27}Al)_0 > 10^{-5}$. While the PDF of published OC chondrules reveals a major peak in initial $^{26}Al/^{27}Al$ at ~7.5×10^{-6}, the new dataset shows two peaks around ~5.5×10^{-6} and 7.5×10^{-6}. A third weaker peak at ~9×10^{-6} is recorded in the dataset from this study as well as very weakly in the previously published data (Fig. 7a). Another less strong cluster of samples with $(^{26}Al/^{27}Al)_0$ ~1.1×10^{-5} for published OC chondrules is not present in the new data which all record $(^{26}Al/^{27}Al)_0 < 10^{-5}$. Combining all OC ferromagnesian chondrule data, two major clusters at 7.5×10^{-6} and 5.5×10^{-6} and possible two less pronounced ones at 9×10^{-6} and 1.1×10^{-5} can be defined that correspond to relative ages of 1.6, 1.8, 2.0 and 2.3 Ma after the formation of CAIs. The data compilation of CC ferromagnesian chondrules includes only a single chondrule with initial $^{26}Al/^{27}Al > 10^{-5}$. Chondrules from Renazzo-type (CR) chondrites record systematically lower $(^{26}Al/^{27}Al)_0$ compared to chondrules from CO and CV chondrites (Nagashima et al., 2008; Nagashima et al., 2014; Schrader et al., 2017) and are therefore treated separately in the density distribution plots (Fig. 7). The PDF of chondrules from CO, CV and ungrouped Acfer094 meteorites shows a major broad peak around $(^{26}Al/^{27}Al)_0 = 5.5 \times 10^{-6}$, whereas chondrules from CR meteorites record three distinct peaks at 6.5×10^{-6}, 3×10^{-6} and 1.5×10^{-6}. When compared to OC chondrules, the highest initial $^{26}Al/^{27}Al$ in CO, CV and Acfer094 chondrules are slightly shifted towards lower values and respective younger dates, while the total recorded range for both chondrite classes is similar (Fig. 7a). The adaptive kernel density estimations (Fig. 7b) do not take into account the analytical uncertainties but vary the bandwidth according to the local density which allows a higher resolution in those parts of the dataset that have the most data points. The KDE of published OC chondrules records two peaks in $(^{26}Al/^{27}Al)_0$ at 1.1×10^{-5} and 7×10^{-6} while the data from this study reveal a single peak at 5.5×10^{-6}. The KDE of the combined data for all chondrules from OC meteorites yields a close to normal distribution around 6.5×10^{-6}. The two statistical approaches yield slightly differing apparent results that can be interpreted differently in the context of chondrule formation. The PDFs reveal more discrete peaks, especially when the dataset is small (e.g. CR chondrites). This involves the risk, that few highly precise ages strongly impact upon the probability density distribution which could lead to an overinterpretation of apparent age peaks. Nevertheless, the KDEs as well as PDFs of OC and CC chondrules reveal a rapid onset in chondrule formation that peaks between 2.0 to 2.3 Ma. Both statistical approaches also suggest that the onset of chondrules formation in most CC groups lightly postdates the onset of chondrule formation in OCs.

5.2.3 Chondrule forming regions and accretion of the chondrite parent bodies

Molybdenum, Ti and Cr isotopes suggest that ordinary and carbonaceous chondrites formed in distinct reservoirs (Warren, 2011; Budde et al., 2016). Chemical complementary between matrix and chondrules (Hezel and Palme, 2010; Palme et al., 2015; Budde et al, 2016) require their formation from common reservoirs, making chondrule transportation over long distances after their formation unlikely. The sharp distinction in bulk meteorite Mo isotopes between the two reservoirs together with isotopic complementarity of chondrules and matrix indicate that most chondrules formed after the chemical dichotomy was achieved in the reservoirs. Recently it has been suggested that the early formed Jupiter could have cleared out the disk and effectively separated the carbonaceous from the noncarbonaceous reservoir (Kruijer et al., 2017). Many studies propose chondrule formation by collision of molten (e.g. Asphaug et al., 2011) or unmolten (e.g. Johnson et al., 2015) planetesimals. While these models are indeed able to describe some essential physical and textural preconditions evident from the meteorite record, they are otherwise difficult to bring into accordance with many chemical characteristics particularly the chemical and isotopic complementarity between chondrules and matrix.

The occurrence of chondrules with distinct ages in single chondrite samples indicates that some older chondrules remained unaffected by later thermal events when younger chondrules formed. This indicates that the chondrule forming process was spatially limited to certain regions in the respective reservoir at a given time. A recent study by Desch et al. (in press) modelling the early separation of the inner from the outer disk by Jupiter suggests surface density maxima in the carbonaceous and noncarbonaceous reservoirs just at the inner and outer edges of Jupiter's orbit. These gas densities would be sufficient to locally process chondrule precursors in bow shocks around planetesimals or planetary embryos. Once Jupiter grew big enough it could have affected the eccentricities of embryos and likely scattered them with supersonic velocity into the density enriched regions. The proximity of these potential chondrule forming reservoirs to the orbit of Jupiter could thus have increased the likelihood of chondrule formation in bow shocks and is consistent with the similar formation periods of OC and CC chondrules as suggested by ^{26}Al-^{26}Mg chronometry. In contrast, early formation of chondrules as suggested by the Pb-Pb system would be difficult to explain in this scenario.

Chondrule formation from 1.8 to 3.0 Ma after CAI requires storage of some chondrules over nearly 1.2 Myr in distinct and closed reservoirs prior to their final accretion into the respective parent bodies. This is consistent with estimated precompaction exposure ages less than a few Ma derived from nuclear track densities and cosmic ray exposure ages of chondrules from L and LL chondrites (Roth et al., 2016). Age constraints on the accretion of the ordinary chondrite parent bodies are sparse. While Hf-W ages of H5 chondrites, which date the cooling of these samples below the closure temperature of the Hf-W system, indicate accretion of the H chondrite parent body before 5.9±0.9 Ma (Kleine et al., 2008), Sugiura and Fujiya (2014) estimated the accretion of the OC parent bodies to ~2.1 Ma after CAIs. By definition, the start of the ordinary chondrite parent body accretion is constrained by the first peak in chondrule formation at ca. 2 Ma after CAIs and the final accretion cannot predate the formation of the youngest chondrules. This constrains the final stage of chondrite parent body accretion to $>2.92^{+0.75}_{-0.43}$ Ma after CAIs.

6. Conclusions

The ^{26}Al-^{26}Mg mineral isochron ages obtained by SIMS for 31 ferromagnesian chondrules from seven least metamorphosed unequilibrated ordinary chondrites of petrologic type<3.15 date the time of melt formation and thus chondrule formation or remelting of pre-existing chondrules. This study comprises the largest data set of Mg isotope systematics in single chondrules from UOCs and extends the existing number of chondrule ^{26}Al-^{26}Mg ages significantly. The initial ^{26}Al/^{27}Al derived from the analyses of olivine, pyroxene and mesostasis range from $(9.5 \pm 2.8) \times 10^{-6}$ to $(3.1 \pm 1.2) \times 10^{-6}$. These ratios correspond to ^{26}Al-^{26}Mg ages from $1.76^{+0.36}_{-0.27}$ Ma to $2.92^{+0.51}_{-0.34}$ Ma after CAI formation using the canonical ^{26}Al/^{27}Al = 5.23×10^{-5}. The chondrule ages are consistent with those determined with different decay schemes based on short-lived isotopes (e.g. ^{182}Hf-^{182}W, ^{53}Mn-^{53}Cr) on other chondritic meteorites, albeit have generally higher precisions. The ages also widely agree with published ^{26}Al-^{26}Mg ages for chondrules from other chondrite samples, although no chondrule was found in this study that records $(^{26}Al/^{27}Al)_0 > 10^{-5}$. The only significantly older ages for chondrules were obtained with the Pb-Pb system by leaching of individual large chondrules, that are unusual and rare in meteorites, and might have been affected by ^{222}Rn loss.

The combination of the new ^{26}Al-^{26}Mg ages presented here with published ^{26}Al-^{26}Mg ages from the literature reveals a narrow age range for chondrule formation that is similar for chondrules from L and LL OCs and CO and CV meteorites. Thus, the dichotomy between the two classes is not expressed in the formation ages of the chondrules but only in their chemical and isotopic differences. The oldest chondrules in the L(LL) and LL chondrites yield a weighted mean age of $1.99^{+0.08}_{-0.08}$ Ma, while the oldest chondrules in the L chondrite samples agree within their 1σ uncertainties with a weighted mean age of $1.81^{+0.11}_{-0.10}$ Ma which is slightly younger but not resolved from the L(LL) and LL chondrite mean age. The oldest chondrules from six of the seven studied UOCs agree within 2σ uncertainty. Chondrule ages range up to ~3.0 Ma after CAIs with apparent age peaks at 2.0 and 2.3 Ma as revealed by PDFs. This reflects protracted chondrule formation and/or reprocessing over a maximum of 1.2 Ma; including the few published older ^{26}Al-^{26}Mg ages, the time interval of chondrule formation extends to ca. 1.5 Ma. The youngest chondrule ages may represent thermal reprocessing of older chondrules or low-temperature alteration of mesostasis prior to accretion into parent bodies.

The mean age of the oldest chondrules in the L chondrite samples is interpreted to record the major and relatively punctuated onset of chondrule formation around $1.81^{+0.11}_{-0.10}$ Ma after formation of CAIs. This indicates that chondrules formed relatively late in the protoplanetary disk after the parent bodies of iron meteorites had formed and differentiated. Thus, chondrules, chondrites and their respective parent bodies are probably not the building blocks but rather the result of early formed planetesimals.

Chondrules from CO and CV and ordinary chondrites formed at similar times and over similar time scales, whereas chondrules from Renazzo-type (CR) meteorites record systematically younger ages. The chemical and Mo-isotopic complementarity of chondrules and their associated matrix in the different chondrite groups requires that chondrules formed from chemically distinct and closed reservoirs. These reservoirs may have been separated by the early formed Jupiter opening a gap in the disk that inhibited efficient mixing prior to the last chondrule forming event. Planetesimals or planetary embryos in the disk that also contains regions of dispersed dust and gas could be an efficient source for bow shocks that caused chondrule formation by melting of pre-existing dust agglomerates. Multiple shocks over a period of ca. 1.2 Myr may have caused reprocessing or remelting of chondrules prior to their incorporation in the respective parent bodies later than ~2.5 to 3.0 Myr after formation of CAIs.

Acknowledgements

We would like to thank the ANSMET meteorite working group (MWG) for providing the samples MET 96503, MET 00452, MET 00526 and QUE 97008 from the NASA Collection of Antarctic Meteorites. We also thank the Natural History Museum, Vienna; Dept. of Mineralogy and Petrography for providing a piece of Eagle Station pallasite olivine. B. Hofmann from the Natural History Museum Bern is acknowledged for providing San Carlos olivine and for discussion on Rn emanation from meteorites. We also thank F. Planet and G. Siron from the SwissSIMS laboratory for their support and helpful discussions during SIMS work. Peter Ulmer is thanked for his help with glass synthesis experiments. Å. V. Rosén is acknowledged for constructive discussion throughout the work on the manuscript.

Constructive reviews by N. Kita, K. Nagashima and one anonymous reviewer improved the quality of this manuscript. M. Boyet is thanked for the editorial handling of the manuscript.

This work has been carried out in the framework of the NCCR PlanetS supported by the Swiss National Science Foundation grant nr. 51NF40-141881. The authors acknowledge the financial support of the SNSF.

References

Alexander C. O. D., Grossman J. N., Wang J., Zanda B., Bourot-Denise M. and Hewins R. H. (2000) The lack of potassium-isotopic fractionation in Bishunpur chondrules. *Meteorit. Planet. Sci* **35**, 859-868.

Amelin Y., Krot A. N., Hutcheon I. D. and Ulyanov A. A. (2002) Lead isotopic ages of chondrules and calcium-aluminum-rich inclusions. *Science* **297**, 1678-1683.

Amelin Y. and Krot A. (2007) Pb isotopic age of the Allende chondrules. *Meteorit. Planet. Sci.* **42**, 1321-1335.

Armstrong J. T. (1995) Citzaf-a package of correction programs for the quantitative Electron Microbeam X-Ray-Analysis of thick polished materials, thin-films, and particles. *Microbeam Anal.* **4**, 177-200.

Asphaug E., Jutzi M. and Movshovitz N. (2011) Chondrule formation during planetesimal accretion. *Earth Planet. Sci. Lett.* **308**, 369-379.

Baecker B., Rubin A. E. and Wasson J. T. (2017) Secondary melting events in Semarkona chondrules revealed by compositional zoning in low-Ca pyroxene. *Geochim. Cosmochim. Acta* **211**, 256-279.

Becker M., Hezel D. C., Schulz T., Elfers B. M. and Münker C. (2015) Formation timescales of CV chondrites from component specific Hf–W systematics. *Earth Planet. Sci. Lett.* **432**, 472-482.

Bizzarro M., Baker J. A. and Haack H. (2004) Mg isotope evidence for contemporaneous formation of chondrules and refractory inclusions. *Nature* **431**, 275.

Bollard J., Connelly J. N., Whitehouse M. J., Pringle E. A., Bonal L., Jørgensen J. K., Nordlund Å, Moynier F. and Bizzarro M. (2017) Early formation of planetary building blocks inferred from Pb isotopic ages of chondrules. Sci. Adv. 3, e1700407.

Bouvier A. and Wadhwa M. (2010) The age of the Solar System redefined by the oldest Pb–Pb age of a meteoritic inclusion. *Nat. Geosci.* **3**, 637.

Budde G., Burkhardt C., Brennecka G. A., Fischer-Gödde M., Kruijer T. S. and Kleine T. (2016) Molybdenum isotopic evidence for the origin of chondrules and a distinct genetic heritage of carbonaceous and non-carbonaceous meteorites. *Earth Planet. Sci. Lett.* **454**, 293-303.

Budde G., Kleine T., Kruijer T. S., Burkhardt C. and Metzler K. (2016) Tungsten isotopic constraints on the age and origin of chondrules. *Proc. Natl. Acad. Sci.* **113**, 2886-2891.

Budde G., Kruijer T. S. and Kleine T. (2018) Hf-W chronology of CR chondrites: Implications for the timescales of chondrule formation and the distribution of 26Al in the solar nebular. *Geochim. Cosmochim. Acta* **222**, 284-304.

Connelly J. N. and Bizzarro M. (2009) Pb–Pb dating of chondrules from CV chondrites by progressive dissolution. *Chem. Geol.* **259**, 143-151.

Connelly J. N., Bizzarro M., Krot A. N., Nordlund Å., Wielandt D. and Ivanova M. A. (2012) The absolute chronology and thermal processing of solids in the solar protoplanetary disk. *Science* **338**, 651-655.

Connelly J. N., Bollard J. and Bizzarro M. (2017) Pb–Pb chronometry and the early solar system. *Geochim. Cosmochim. Acta* **201**, 345-363.

Davis A. M., Richter F. M., Mendybaev R. A., Janney P. E., Wadhwa M. and McKeegan K. D. (2015) Isotopic mass fractionation laws for magnesium and their effects on ^{26}Al–^{26}Mg systematics in solar system materials. *Geochim. Cosmochim. Acta* **158**, 245-261.

Desch S. J. and Cuzzi J. N. (2000) The generation of lightning in the solar nebula. *Icarus* **143**, 87-105.

Desch S. J., and Connolly H. C. (2002) A model of the thermal processing of particles in solar nebula shocks: Application to the cooling rates of chondrules. *Meteorit. Planet. Sci.* ***37***, 183-207.

Desch S. J., Kalyaan A. and Alexander C. M. D. (2017) The Effect of Jupiter's Formation on the Distribution of Refractory Elements and Inclusions in Meteorites. *Astrophys. J. Supplement (in press)*.

Eakin M., Brownlee S. J., Baskaran M. and Barbero L. (2016) Mechanisms of radon loss from zircon: microstructural controls on emanation and diffusion. *Geochim. Cosmochim. Acta* **184**, 212-226.

Girault F., Perrier F., Moreira M., Zanda B., Rochette P. and Teitler Y. (2017) Effective radium-226 concentration in meteorites. *Geochim. Cosmochim. Acta* **208**, 198-219.

Grossman J. N. and Brearley A. J. (2005). The onset of metamorphism in ordinary and carbonaceous chondrites. *Meteorit. Planet. Sci.* **40**, 87-122.

Hewins R. H., and Connolly H. C., Jr. (1996) Peak temperatures of flash-melted chondrules. In *Chondrules and the Protoplanetary Disk* (ed. R. H. Hewins et al.), pp. 197-204. Cambridge Univ. Press.

Hezel D. C. and Palme H. (2010) The chemical relationship between chondrules and matrix and the chondrule matrix complementarity. *Earth Planet. Sci. Lett.* **294**, 85-93.

Hutcheon I. D. and Hutchison R. (1989) Evidence from the Semarkona ordinary chondrite for ^{26}Al heating of small planets. *Nature* **337**, 238-241.

Hutcheon I. D., Krot A. N. and Ulyanov A. A. (2000) ^{26}Al in anorthite-rich chondrules in primitive carbonaceous chondrites: evidence chondrules postdate CAI. In *Lunar Planet. Sci. Conf.* (Vol. 31).

Jacobsen B., Yin, Q. Z., Moynier F., Amelin Y., Krot A. N., Nagashima K., Hutcheon I. D. and Palme, H. (2008) ^{26}Al–^{26}Mg and ^{207}Pb–^{206}Pb systematics of Allende CAIs: Canonical solar initial ^{26}Al/^{27}Al ratio reinstated. *Earth Planet. Sci. Lett.* **272**, 353-364.

Johansen A., Low M.-M. M., Lacerda P. and Bizzarro M. (2015) Growth of asteroids, planetary embryos, and Kuiper belt objects by chondrule accretion. *Sci. Adv.* **1**, e1500109.

Johnson B. C., Minton D. A., Melosh H. J. and Zuber M. T. (2015) Impact jetting as the origin of chondrules. *Nature* **517**, 339.

Jones R. H. and Scott E. R. D. (1989) Petrology and thermal history of type IA chondrules in the Semarkona (LL3. 0) chondrite. *Proc. 19th Lunar Planet. Sci. Conf.*, 523-536.

Jones R. H., Grossman J. N. and Rubin A. E. (2005) Chemical, mineralogical and isotopic properties of chondrules: Clues to their origin. In *Chondrites and the Protoplanetary Disk,* vol. 341 (eds. A. N. Krot, E. R. D. Scott and B. Reipurth). *ASP Conference Series*, pp. 251-286.

Kita N. T., Nagahara H., Togashi S. and Morishita Y. (2000) A short duration of chondrule formation in the solar nebula: Evidence from ^{26}Al in Semarkona ferromagnesian chondrules. *Geochim. Cosmochim. Acta* **64**, 3913-3922.

Kita N. T., Tomomura S., Tachibana S., Nagahara H., Mostefaoui S. and Morishita Y. (2005) Correlation between aluminum-26 ages and bulk Si/Mg ratios for chondrules from LL3.0-3.1 chondrites. *Lunar Planet. Sci. Conf.* **36**, #1750 (abstr.).

Kita N. T. and Ushikubo T. (2012) Evolution of protoplanetary disk inferred from ^{26}Al chronology of individual chondrules. *Meteorit. Planet. Sci.* **47**, 1108-1119.

Kita N. T., Ushikubo T., Knight K. B., Mendybaev R. A., Davis A. M., Richter F. M. and Fournelle J. H. (2012) Internal ^{26}Al–^{26}Mg isotope systematics of a Type B CAI: remelting of refractory precursor solids. *Geochim. Cosmochim. Acta* **86**, 37-51.

Kita N. T., Yin Q. Z., MacPherson G. J., Ushikubo T., Jacobsen B., Nagashima K., Kurahashi E., Krot A. N., and Jacobsen S. B. (2013) ^{26}Al-^{26}Mg isotope systematics of the first solids in the early solar system. *Meteorit. Planet. Sci.* **48**, 1383-1400.

Kita N. T., Tenner T. J., Ushikubo T., Bouvier A., Wadhwa M., Bullock E. S. and MacPherson G. J. (2015) Why do U-Pb ages of chondrules and CAIs have more spread than their ^{26}Al ages? *Meteorit. Planet. Sci.* **78,** #5360 (abstr.).

Kleine T., Touboul M., Van Orman J. A., Bourdon B., Maden C., Mezger K. and Halliday A. N. (2008) Hf–W thermochronometry: closure temperature and constraints on the accretion and cooling history of the H chondrite parent body. *Earth Planet. Sci. Lett.* **270**, 106-118.

Krot A. N., Fagan T. J., Keil K., McKeegan K. D., Sahijpal S., Hutcheon I. D., Petaev M. I. and Yurimoto H. (2004). Ca, Al-rich inclusions, amoeboid olivine aggregates, and Al-rich chondrules from the unique carbonaceous chondrite Acfer 094: I. Mineralogy and petrology. *Geochim. Cosmochim. Acta* **68**, 2167-2184.

Krot A. N., Amelin Y., Cassen P. and Meibom A. (2005) Young chondrules in CB chondrites from a giant impact in the early Solar System. *Nature* **436**, 989.

Kruijer T. S., Kleine T., Fischer-Gödde M., Burkhardt, C. and Wieler R. (2014) Nucleosynthetic W isotope anomalies and the Hf–W chronometry of Ca–Al-rich inclusions. *Earth Planet. Sci. Lett.* **403** 317-327.

Kruijer T. S., Burkhardt C., Budde G. and Kleine T. (2017) Age of Jupiter inferred from the distinct genetics and formation times of meteorites. *Proc. Natl. Acad. Sci.* **114**, 6712-6716.

Kunihiro T., Rubin A. E., McKeegan K. D. and Wasson J. T. (2004). Initial ^{26}Al/^{27}Al in carbonaceous-chondrite chondrules: too little ^{26}Al to melt asteroids. *Geochim. Cosmochim. Acta* **68**, 2947-2957.

Kurahashi E., Kita N. T., Nagahara H. and Morishita Y. (2008) ^{26}Al–^{26}Mg systematics of chondrules in a primitive CO chondrite. *Geochim. Cosmochim. Acta* **72**, 3865-3882.

Lanari P., Vidal O., De Andrade V., Dubacq B., Lewin E., Grosch E. G. and Schwartz S. (2014) XMapTools: A MATLAB©-based program for electron microprobe X-ray image processing and geothermobarometry. *Comp. Geosci.* **62**, 227-240.

Larsen K. K., Trinquier A., Paton C., Schiller M., Wielandt D., Ivanova M. A., Connelly J. N., Nordlund Å., Krot A. N. and Bizzarro M. (2011) Evidence for magnesium isotope heterogeneity in the solar protoplanetary disk. *Astrophys. J. Lett.* **735**, L37.

Larsen K. K., Schiller M. and Bizzarro M. (2016) Accretion timescales and style of asteroidal differentiation in an 26Al-poor protoplanetary disk. *Geochim. Cosmochim. Acta* 176, 295–315.

Lichtenberg T., Golabek G. J., Dullemond C. P., Schönbächler M., Gerya T. V. and Meyer, M. R. (2018) Impact splash chondrule formation during planetesimal recycling. *Icarus* **302**, 27-43.

Liu M. C., Chaussidon M., Göpel C. and Lee T. (2012) A heterogeneous solar nebula as sampled by CM hibonite grains. *Earth Planet. Sci. Lett.* **327**, 75-83.

Liu M. C., McKeegan K. D., Harrison T. M., Jarzebinski G. and Vltava L. (2018) The Hyperion-II radio-frequency oxygen ion source on the UCLA ims1290 ion microprobe: Beam characterization and applications in geochemistry and cosmochemistry. *Int. J. Mass Spectrom.* **424**, 1-9.

Ludwig K. R. (2003) User's manual for Isoplot 3.00: a geochronological toolkit for Microsoft Excel (No. 4). Berkeley Geochronology Centre, Special Publication.

Luu T. H., Chaussidon M., Mishra R. K., Rollion-Bard C., Villeneuve J., Srinivasan G. and Birck J. L. (2013) High precision Mg isotope measurements of meteoritic samples by secondary ion mass spectrometry. *J. Analyt. Atom. Spectrom.* **28**, 67-76.

Luu T. H., Young E. D., Gounelle M. and Chaussidon M. (2015) Short time interval for condensation of high-temperature silicates in the solar accretion disk. *Proc. Natl. Acad. Sci.* **112**, 1298-1303.

Makide K., Nagashima K., Krot A. N., Huss G. R., Ciesla F. J., Hellebrand E., Gaidos E and Yang L. (2011) Heterogeneous distribution of ^{26}Al at the birth of the solar system. *Astrophys. J. Lett.* **733**, L31-L34.

MacPherson G. J., Davis A. M. and Zinner E. K. (1995) The distribution of aluminum-26 in the early Solar System—A reappraisal. *Meteorit. Planet. Sci.* **30**, 365-386.

MacPherson G. J., Bullock E. S., Tenner T. J., Nakashima D., Kita N. T., Ivanova M. A., Krot A. N., Petaev M. I. and Jacobsen S. B. (2017). High precision Al–Mg systematics of forsterite-bearing Type B CAIs from CV3 chondrites. *Geochim. Cosmochim. Acta*, **201**, 65-82.

Metzler K. (2018) From 2D to 3D chondrule size data: Some empirical ground truths. *Meteorit. Planet. Sci.* https://doi.org/10.1111/maps.13091

Mishra R. K. and Chaussidon M. (2014) Timing and extent of Mg and Al isotopic homogenization in the early inner Solar System. *Earth Planet. Sci. Lett.* **390**, 318-326.

Morris M. A., Boley A. C., Desch S. J. and Athanassiadou T. (2012) Chondrule formation in bow shocks around eccentric planetary embryos. *Astrophys. J.* **752**, 27.

Mostefaoui S., Kita N. T., Togashi S., Tachibana S., Nagahara H. and Morishita Y. (2002) The relative formation ages of ferromagnesian chondrules inferred from their initial aluminum-26/aluminum-27 ratios. *Meteorit. Planet. Sci.* **37**, 421-438.

Nagashima K., Krot A. N. and Chaussidon M. (2007) Aluminum-magnesium isotope systematics of chondrules from CR chondrites. *Meteorit. Planet. Sci.*, **42**, #5291 (abstr.).

Nagashima K., Krot A. N., & Huss G. R. (2008) ^{26}Al in chondrules from CR carbonaceous chondrites. *Lunar Planet. Sci.* **39**, #2224 (abstr.).

Nagashima K., Krot A. N. and Huss G. R. (2014) 26Al in chondrules from CR2 chondrites. *Geochem. J.* 48, 561–570.

Nagashima K., Krot A. N. and Komatsu M. (2017) ^{26}Al-^{26}Mg systematics in chondrules from Kaba and Yamato 980145 CV3 carbonaceous chondrites. *Geochim. Cosmochim. Acta* **201**, 303-319.

Palme H., Hezel D. C. and Ebel D. S. (2015) The origin of chondrules: Constraints from matrix composition and matrix-chondrule complementarity. *Earth Planet. Sci. Lett.* **411**, 11-19.

Park C., Nagashima K., Krot A. N., Huss G. R., Davis A. M. and Bizzarro M. (2017) Calcium-aluminum-rich inclusions with fractionation and unidentified nuclear effects (FUN CAIs): II. Heterogeneities of magnesium isotopes and ^{26}Al in the early Solar System inferred from in situ high-precision magnesium-isotope measurements. *Geochim. Cosmochim. Acta* **201**, 6-24.

Rama, Moore W. S. (1984) Mechanism of transport of U-Th series radioisotopes from solids into ground water. *Geochim. Cosmochim. Acta* **48**, 395-399.

Roth A. S., Metzler K., Baumgartner L. P. and Leya I. (2016) Cosmic-ray exposure ages of chondrules. *Meteorit. Planet. Sci.* **51**, 1256-1267.

Rubin A. E. (2010) Physical properties of chondrules in different chondrite groups: Implications for multiple melting events in dusty environments. *Geochim. Cosmochim. Acta* **74**, 4807-4828.

Rudraswami N. G. and Goswami J. N. (2007) ^{26}Al in chondrules from unequilibrated L chondrites: Onset and duration of chondrule formation in the early solar system. *Earth Planet. Sci. Lett.* **257**, 231-244.

Rudraswami N. G., Goswami J. N., Chattopadhyay B., Sengupta S. K. and Thapliyal A. P. (2008) ^{26}Al records in chondrules from unequilibrated ordinary chondrites: II. Duration of chondrule formation and parent body thermal metamorphism. *Earth Planet. Sci. Lett.* **274**, 93-102.

Russell S. S., Krot A. N., Huss G. R., Keil K., Itoh S., Yurimoto H. and MacPherson G. J. (2005) The genetic relationship between refractory inclusions and chondrules. In *Chondrites and the Protoplanetary Disk,* vol. 341 (eds. A. N. Krot, E. R. D. Scott and B. Reipurth). *ASP Conference Series*, pp. 317-353.

Schiller M., Connelly J. N., Glad A. C., Mikouchi T. and Bizzarro M. (2015) Early accretion of protoplanets inferred from a reduced inner solar system ^{26}Al inventory. *Earth Planet. Sci. Lett.* **420**, 45-54.

Schrader D. L., Nagashima K., Krot A. N., Ogliore R. C., Yin Q.-Z., Amelin Y., Stirling C. H. and Kaltenbach A. (2017) Distribution of 26Al in the CR chondrite chondrule-forming region of the protoplanetary disk. *Geochim. Cosmochim. Acta* **201**, 275–302.

Sugiura N. and Krot A. N. (2007) ^{26}Al-^{26}Mg systematics of Ca-Al-rich inclusions, amoeboid olivine aggregates, and chondrules from the ungrouped carbonaceous chondrite Acfer 094. *Meteorit. Planet. Sci.* **42**, 1183-1195.

Sugiura N. and Fujiya W. (2014). Correlated accretion ages and ε54Cr of meteorite parent bodies and the evolution of the solar nebula. *Meteorit. Planet. Sci.* **49**, 772-787.

Teng F. Z., Li W. Y., Ke S., Marty B., Dauphas N., Huang S., Wu F. Y. and Pourmand A. (2010) Magnesium isotopic composition of the Earth and chondrites. *Geochim. Cosmochim. Acta* **74**, 4150-4166.

Ushikubo T., Kimura M., Nakashima D. and Kita N. T. (2010) A combined study of the Al-Mg systematics and O isotope ratios of chondrules from the primitive carbonaceous chondrite Acfer 094. *Lunar Planet. Sci. Conf.* **41**, #1491 (abstr.).

Ushikubo T., Nakashima D., Kimura M., Tenner T. J. and Kita N. T. (2013). Contemporaneous formation of chondrules in distinct oxygen isotope reservoirs. *Geochim. Cosmochim. Acta*, **109**, 280-295.

Vermeesch P. (2012) On the visualisation of detrital age distributions. *Chem. Geol.* **312–313**, 190–194.

Villeneuve J., Chaussidon M. and Libourel G. (2009) Homogeneous distribution of 26Al in the solar system from the Mg isotopic composition of chondrules. *Science* **325**, 985-988.

Villeneuve J., Libourel G. and Soulié C. (2015) Relationships between type I and type II chondrules: Implications on chondrule formation processes. *Geochim. Cosmochim. Acta* **160**, 277-305.

Warren P. H. (2011) Stable-isotopic anomalies and the accretionary assemblage of the Earth and Mars: A subordinate role for carbonaceous chondrites. *Earth Planet. Sci. Lett.* **311**, 93-100.

Wasserburg G. J., Wimpenny J. and YIN Q. Z. (2012) Mg isotopic heterogeneity, Al-Mg isochrons, and canonical ^{26}Al/^{27}Al in the early solar system. *Meteorit. Planet. Sci.* **47**, 1980-1997.

Wasson J. and Kallemeyn G. (1988) Compositions of chondrites. Philos. Trans. R. Soc. A **325**, 535–544.

Wasson J. T. and Rubin A. E. (2003) Ubiquitous low-FeO relict grains in type II chondrules and limited overgrowths on phenocrysts following the final melting event. *Geochim. Cosmochim. Acta* **67**, 2239-2250.

Weisberg M. K., McCoy T. J. and Krot A. N. (2006) Systematics and evaluation of meteorite classification. D.S. Lauretta, H.Y. McSween Jr. (Eds.), Meteorites and the Early Solar System II, The University of Arizona Press (2006), pp. 9-53.

Yang W., Teng F. Z. and Zhang H. F. (2009) Chondritic magnesium isotopic composition of the terrestrial mantle: a case study of peridotite xenoliths from the North China craton. *Earth Planet. Sci. Lett.* **288**, 475-482.

Yin Q. Z., Jacobsen B., Moynier F. and Hutcheon I. D. (2007) Toward consistent chronology in the early solar system: high-resolution ^{53}Mn-^{53}Cr chronometry for chondrules. *Astrophys. J. Lett.* **662**, L43

Youdin A. N., and Shu F. H. (2002) Planetesimal formation by gravitational instability. *Astrophy. J.* **580**, 494.

Yurimoto H. and Wasson J. T. (2002) Extremely rapid cooling of a carbonaceous-chondrite chondrule containing very ^{16}O-rich olivine and a ^{26}Mg-excess. *Geochim. Cosmochim. Acta*, **66**, 4355-4363.

Table 1

Al-Mg isotope data for ferromagnesian chondrules. Initial $^{26}Al/^{27}Al$ and $(\delta^{26}Mg^*)_0$ were calculated from the slope and intercept of isochron regressions using the Isoplot software Model 1 (Ludwig 2003). $\delta^{26}Mg^*$ and $^{27}Al/^{24}Mg$ ratios of single measurements used for regression of isochrons are provided in the Supplement Table S1.

Sample	**Type**	**Meas. phases**	**$^{27}Al/^{24}Mg$ a)**	**$\delta^{26}Mg^*_0$ (‰)**	**$(^{26}Al/^{27}Al)_0$**	**Δt_{CAI} (Ma)**	**Δt_{CAI} (Ma)d)**
MET 96503 L3.10							
MET 96503 Ch2 c)	PO II	7 Mes / 7 Ol	1.6-4.7	-0.003 ± 0.030	(8.0 ± 2.4) × 10^{-6}	$\mathbf{1.94}^{+0.37}_{-0.27}$	$1.96^{+0.25}_{-0.20}$
MET 96503 Ch3	PO II	3 Mes / 6 Ol	2.6-3.1	-0.007 ± 0.026	(4.3 ± 2.3) × 10^{-6}	$\mathbf{2.58}^{+0.79}_{-0.44}$	$2.63^{+0.69}_{-0.41}$
MET 96503 Ch4	PP/POP II	6 Mes / 2 Ol / 2 Px	6.4-68.7	-0.006 ± 0.052	(5.51 ± 0.52) × 10^{-6}	$\mathbf{2.33}^{+0.10}_{-0.09}$	$2.33^{+0.10}_{-0.09}$
MET 96503 Ch8 b)	POP II	6 Mes / 5 Ol	7.9-11.9	-0.007 ± 0.072	(6.2 ± 1.8) × 10^{-6}	$\mathbf{2.21}^{+0.35}_{-0.26}$	$2.22^{+0.13}_{-0.11}$
MET 96503 Ch9	PO II	2 Mes / 4 Ol	3.4-3.6	-0.010 ± 0.029	(5.1 ± 2.3) × 10^{-6}	$\mathbf{2.41}^{+0.62}_{-0.39}$	$2.47^{+0.56}_{-0.36}$
MET 96503 Ch11 c)	PO II	5 Mes / 3 Ol	2.0-2.2	0.002 ± 0.044	(3.7 ± 3.6) × 10^{-6}	$\mathbf{2.74}^{-}_{-0.70}$	$2.69^{+0.74}_{-0.43}$
MET 96503 Ch17 b)	PO/POP II	8 Mes / 9 Ol	5.8-19.5	-0.019 ± 0.058	(9.4 ± 1.5) × 10^{-6}	$\mathbf{1.78}^{+0.18}_{-0.15}$	$1.80^{+0.08}_{-0.08}$
MET 96503 Ch19	PO/POP II	4 Mes / 4 Ol	5.0-7.0	-0.018 ± 0.046	(8.7 ± 1.5) × 10^{-6}	$\mathbf{1.86}^{+0.20}_{-0.16}$	$1.89^{+0.15}_{-0.13}$
MET 96503 Ch28 c)	POP II	4 Mes / 3 Ol	4.8-13.8	0.008 ± 0.040	(3.1 ± 1.2) × 10^{-6}	$\mathbf{2.92}^{+0.51}_{-0.34}$	$2.86^{+0.35}_{-0.26}$
NWA 5206 LL3.05							
NWA 5206 Ch1	PO II	6 Mes / 4 Ol	2.5-3.5	-0.013 ± 0.054	(5.9 ± 2.9) × 10^{-6}	$\mathbf{2.26}^{+0.70}_{-0.41}$	$2.35^{+0.34}_{-0.25}$
NWA 5206 Ch7 b)	PP II	5 Mes / 3 Px	5.5-23.9	-0.019 ± 0.067	(5.4 ± 1.3) × 10^{-6}	$\mathbf{2.35}^{+0.28}_{-0.22}$	$2.39^{+0.12}_{-0.11}$
NWA 5206 Ch8	POP II	4 Mes / 4 Ol / 1 Px	9.7-15.7	0.00 ± 0.03	(7.76 ± 0.82) × 10^{-6}	$\mathbf{1.97}^{+0.12}_{-0.10}$	$1.97^{+0.10}_{-0.09}$
NWA 5206 Ch10	POP II	6 Mes / 4 Ol	4.4-18.7	0.007 ± 0.035	(4.6 ± 1.0) × 10^{-6}	$\mathbf{2.51}^{+0.25}_{-0.20}$	$2.47^{+0.18}_{-0.15}$
NWA 5206 Ch11	POP II	5 Mes / 3 Ol	6.4-13.2	0.008 ± 0.023	(4.07 ± 0.97) × 10^{-6}	$\mathbf{2.64}^{+0.28}_{-0.22}$	$2.61^{+0.25}_{-0.20}$
MET 00526 L(LL)3.05							
MET 00526 Ch1 c)	PO II	5 Mes / 4 Ol	2.2-2.8	0.011 ± 0.037	(6.0 ± 2.6) × 10^{-6}	$\mathbf{2.24}^{+0.59}_{-0.37}$	$2.13^{+0.28}_{-0.22}$
MET 00526 Ch7 b)	POP II	7 Mes / 8 Ol	2.8-12.1	-0.002 ± 0.044	(7.8 ± 1.4) × 10^{-6}	$\mathbf{1.97}^{+0.20}_{-0.17}$	$1.97^{+0.10}_{-0.09}$
MET 00526 Ch8	POP II	3 Mes / 3 Ol	4.7-5.4	0.008 ± 0.043	(5.5 ± 1.7) × 10^{-6}	$\mathbf{2.33}^{+0.38}_{-0.28}$	$2.27^{+0.26}_{-0.21}$
MET 00526 Ch10	POP II	4 Mes / 3 Px	5.8-23.8	0.009 ± 0.038	(7.31 ± 0.90) × 10^{-6}	$\mathbf{2.04}^{+0.14}_{-0.12}$	$2.02^{+0.12}_{-0.11}$
NWA 8276 L3.00							
NWA 8276 Ch1 b)	POP II	9 Mes / 5 Ol	2.1-30.9	-0.006 ± 0.064	(6.8 ± 1.4) × 10^{-6}	$\mathbf{2.11}^{+0.24}_{-0.19}$	$2.13^{+0.09}_{-0.08}$
NWA 8276 Ch2 b)	POP I	6 Mes / 5 Ol	2.9-4.1	0.007 ± 0.072	(-1.2 ± 3.8) × 10^{-6}	**-**	-
NWA 8276 Ch7	PO II	4 Mes / 6 Ol	2.9-5.0	-0.020 ± 0.028	(4.3 ± 1.6) × 10^{-6}	$\mathbf{2.58}^{+0.48}_{-0.33}$	$2.71^{+0.48}_{-0.32}$
NWA 8276 Ch8	PO II	4 Mes / 8 Ol	2.0-3.0	-0.016 ± 0.023	(9.5 ± 2.8) × 10^{-6}	$\mathbf{1.76}^{+0.36}_{-0.27}$	$1.86^{+0.35}_{-0.26}$
NWA 8276 Ch9	PO II	4 Mes / 4 Ol	4.3-6.2	0.002 ± 0.027	(5.8 ± 1.3) × 10^{-6}	$\mathbf{2.27}^{+0.26}_{-0.21}$	$2.26^{+0.21}_{-0.18}$

MET 00452 L(LL)3.05							
MET 00452 Ch14	POP II	4 Mes / 4 Ol	6.1-7.4	-0.017 ± 0.038	$(3.6 \pm 1.4) \times 10^{-6}$	$\mathbf{2.76^{+0.50}_{-0.34}}$	$2.86^{+0.42}_{-0.30}$
MET 00452 Ch21	POP II	4 Mes / 2 Ol	3.9-26.6	0.011 ± 0.039	$(7.34 \pm 0.99) \times 10^{-6}$	$\mathbf{2.03^{+0.15}_{-0.13}}$	$2.01^{+0.13}_{-0.12}$
MET 00452 Ch22	POP I	4 Mes / 4 Px	3.6-6.9	-0.015 ± 0.040	$(3.1 \pm 1.6) \times 10^{-6}$	$\mathbf{2.92^{+0.75}_{-0.43}}$	$3.07^{+0.54}_{-0.35}$
MET 00452 Ch23 [b)]	PP II	6 Mes / 5 Px	5.2-16.0	-0.016 ± 0.048	$(5.0 \pm 1.4) \times 10^{-6}$	$\mathbf{2.43^{+0.34}_{-0.26}}$	$2.49^{+0.16}_{-0.14}$
QUE 97008 L3.05							
QUE 97008 Ch8	POP II	5 Mes / 2 Ol / 1 Px	6.4-7.0	0.019 ± 0.059	$(5.6 \pm 1.6) \times 10^{-6}$	$\mathbf{2.31^{+0.35}_{-0.26}}$	$2.24^{+0.19}_{-0.16}$
QUE 97008 Ch9	POP II	2 Mes / 1 Ol / 1 Px	6.6-21.2	0.007 ± 0.069	$(8.8 \pm 1.3) \times 10^{-6}$	$\mathbf{1.84^{+0.16}_{-0.14}}$	$1.83^{+0.14}_{-0.12}$
QUE 97008 Ch13	POP II	4 Mes / 2 Ol	6.8-9.9	-0.012 ± 0.070	$(6.4 \pm 1.6) \times 10^{-6}$	$\mathbf{2.16^{+0.29}_{-0.23}}$	$2.19^{+0.18}_{-0.15}$
NWA 7936 L3.15							
NWA 7936 Ch2	PP II	3 Mes / 5 Px	9.8-13.5	0.002 ± 0.033	$(4.8 \pm 1.2) \times 10^{-6}$	$\mathbf{2.47^{+0.30}_{-0.23}}$	$2.45^{+0.26}_{-0.21}$

Unless marked differently errors are 2σ, Abbreviations: Mes, mesostasis; Ol, olivine, Px, pyroxene

a) Range of Al/Mg in mesostasis, **b)** 95% Confidence-limit, **c)** at least single mesostasis measurements from the isochron regression of this chondrule contain high amounts of high-Ca pyroxene dendrites, see *2.1.2,* d) ^{26}Al-^{26}Mg model ages calculated from isochron regressions that were constructed by using all olivine and pyroxene measurements combined from this study for each chondrule.

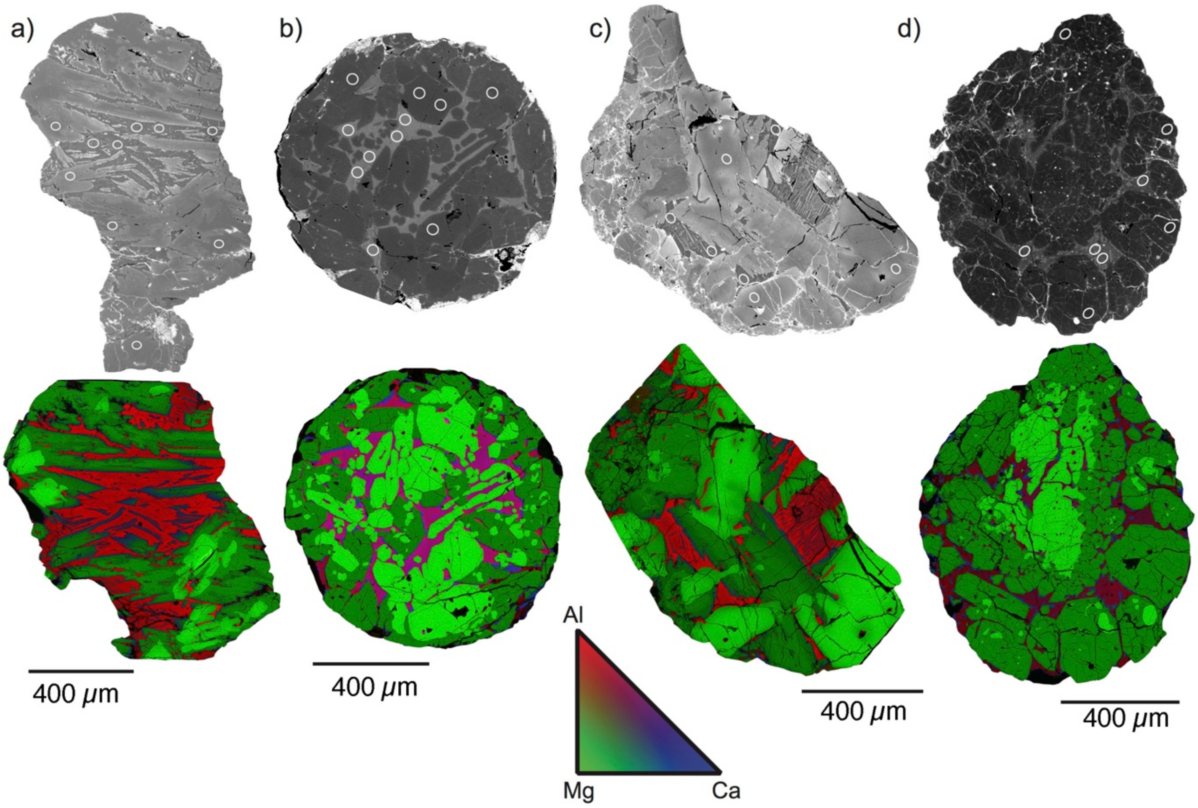

Fig. 1. Backscattered electron (BSE) images and element maps (EPMA) of four chondrules (a) MET96503_Ch4, (b) NWA8276_Ch2, (c) MET96503_Ch28 and (d) MET00452_Ch22. Elemental maps are three-channel composite images, generated from element counts for Al (red), Mg (green) and Ca (blue) using XMapTools 2.3.1 software (Lanari et al. 2014). Light-green colours correspond to olivine, dark-green colours correspond to low-Ca pyroxene and reddish colours to mesostasis. Some chondrules display high-Ca pyroxene crystals (blue). The purple colour of mesostasis in (b) and (d) indicates elevated Ca concentration in mesostasis of type-I chondrules. The white circles in the BSE images indicate where the SIMS measurements were obtained. BSE images and chemical maps do not sample the identical cuts across the chondrules due to repolishing between analyses.

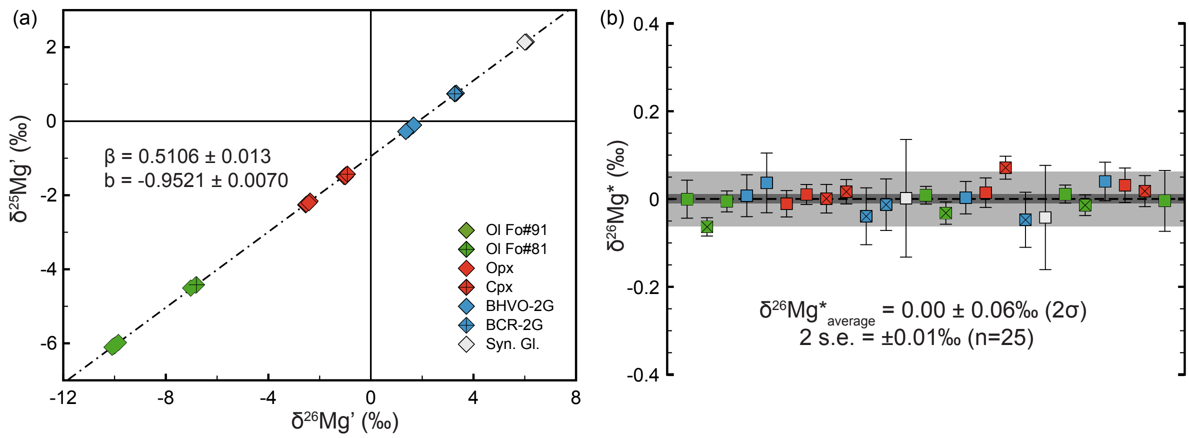

Fig. 2. (a) Three-isotope diagram for δ^{25}Mg' vs. δ^{26}Mg' showing the instrumental mass fractionation law determined during a single session from measurements of seven reference materials. (b) Resulting δ^{26}Mg* for the same measurements as shown in (a) after correction for IMF. The light grey field indicates the 2σ uncertainty on the mean δ^{26}Mg* of all standard measurements. 2 SE for individual measurements in (a) are within symbol size. Error bars in (b) are 2σ.

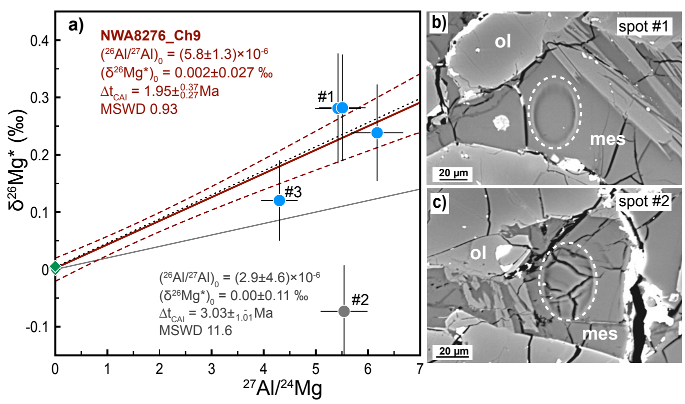

Fig. 3. The impact of a poor quality sample surface (i.e. cracks) and high-Ca pyroxene dendrites on SIMS analysis exemplified with sample NWA8276_Ch9 (a). Using all SIMS measurements i.e. including spot #2 (c) measured in highly fractured mesostasis for the isochron regression, the resulting isochron (grey solid line) is biased towards lower $(^{26}Al/^{27}Al)_0$ of 2.9 ± 4.6 x 10^{-6}, has a large error (error envelope is not shown for the sake of clarity) and a high MSDW of 11.6. The correct isochron (red solid line) includes only measurements with appropriate sample surface (e.g. spot #1 (b)). Spot #3 contained very minor amounts of high-Ca pyroxene dendrites, but this does not bias the isochron regression, because excluding spot #3 changes the isochron only slightly towards higher $(^{26}Al/^{27}Al)_0$ (black dotted line, within the error of the

original isochron) and would shift the relative age (Δt_{CAI}) by less than 80 000 yrs. ol: olivine; mes: mesostasis.

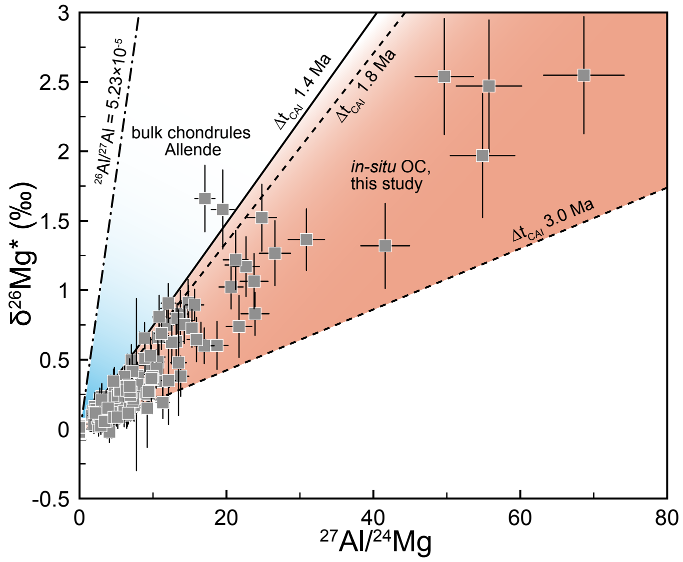

Fig. 4. All Al-Mg isotope measurements of this study plotted in the ^{26}Al-^{27}Al evolution diagram (grey squares). The blue field corresponds to the range (in (^{26}Al/^{27}Al)$_0$ space) of bulk ferromagnesian and Al-rich chondrules from the CV Allende meteorite (Bizzarro et al., 2004; Luu et al., 2015) that can be interpreted to record minimum formation ages of chondrule precursor material by chemical fractionation from a chondritic reservoir. The orange field corresponds to the majority of published ^{26}Al-^{26}Mg in-situ mineral isochron data from CC and OC chondrules. The solid line indicates the isochron for the youngest bulk chondrule model age of ~1.4 Ma (Bizzarro et al., 2004) and the two dashed lines represent the oldest and youngest mineral isochron ages from this study of ~1.8 and ~3.0 Ma, respectively, assuming a homogeneous distribution of ^{26}Al in the protoplanetary disk.

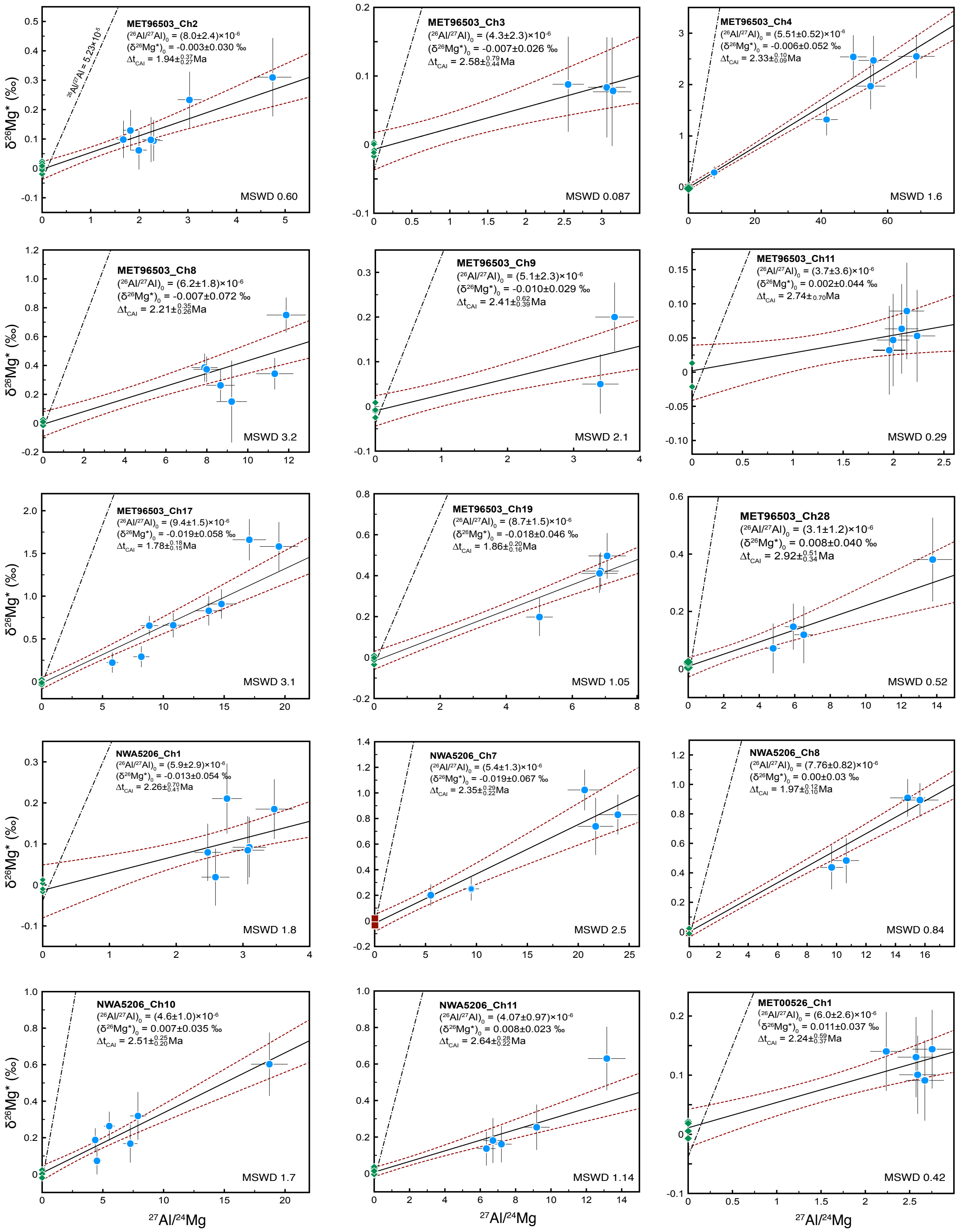

MET96503_Ch2
(26Al/27Al)0 = (8.0±2.4)×10-6
(δ26Mg*)0 = -0.003±0.030 ‰
ΔtCAI = 1.94+0.37-0.27Ma
26Al/27Al = 5.23×10-5
MSWD 0.60
MET96503_Ch3
(26Al/27Al)0 = (4.3±2.3)×10-6
(δ26Mg*)0 = -0.007±0.026 ‰
ΔtCAI = 2.58+0.79-0.44Ma
MSWD 0.087
MET96503_Ch4
(26Al/27Al)0 = (5.51±0.52)×10-6
(δ26Mg*)0 = -0.006±0.052 ‰
ΔtCAI = 2.33+0.10-0.09Ma
MSWD 1.6
MET96503_Ch8
(26Al/27Al)0 = (6.2±1.8)×10-6
(δ26Mg*)0 = -0.007±0.072 ‰
ΔtCAI = 2.21+0.35-0.26Ma
MSWD 3.2
MET96503_Ch9
(26Al/27Al)0 = (5.1±2.3)×10-6
(δ26Mg*)0 = -0.010±0.029 ‰
ΔtCAI = 2.41+0.62-0.39Ma
MSWD 2.1
MET96503_Ch11
(26Al/27Al)0 = (3.7±3.6)×10-6
(δ26Mg*)0 = 0.002±0.044 ‰
ΔtCAI = 2.74±0.70Ma
MSWD 0.29
MET96503_Ch17
(26Al/27Al)0 = (9.4±1.5)×10-6
(δ26Mg*)0 = -0.019±0.058 ‰
ΔtCAI = 1.78+0.18-0.15Ma
MSWD 3.1
MET96503_Ch19
(26Al/27Al)0 = (8.7±1.5)×10-6
(δ26Mg*)0 = -0.018±0.046 ‰
ΔtCAI = 1.86+0.20-0.16Ma
MSWD 1.05
MET96503_Ch28
(26Al/27Al)0 = (3.1±1.2)×10-6
(δ26Mg*)0 = 0.008±0.040 ‰
ΔtCAI = 2.92+0.51-0.34Ma
MSWD 0.52
NWA5206_Ch1
(26Al/27Al)0 = (5.9±2.9)×10-6
(δ26Mg*)0 = -0.013±0.054 ‰
ΔtCAI = 2.26+0.70-0.41Ma
MSWD 1.8
NWA5206_Ch7
(26Al/27Al)0 = (5.4±1.3)×10-6
(δ26Mg*)0 = -0.019±0.067 ‰
ΔtCAI = 2.35+0.29-0.22Ma
MSWD 2.5
NWA5206_Ch8
(26Al/27Al)0 = (7.76±0.82)×10-6
(δ26Mg*)0 = 0.00±0.03 ‰
ΔtCAI = 1.97+0.12-0.10Ma
MSWD 0.84
NWA5206_Ch10
(26Al/27Al)0 = (4.6±1.0)×10-6
(δ26Mg*)0 = 0.007±0.035 ‰
ΔtCAI = 2.51+0.25-0.20Ma
MSWD 1.7
NWA5206_Ch11
(26Al/27Al)0 = (4.07±0.97)×10-6
(δ26Mg*)0 = 0.008±0.023 ‰
ΔtCAI = 2.64+0.28-0.22Ma
MSWD 1.14
MET00526_Ch1
(26Al/27Al)0 = (6.0±2.6)×10-6
(δ26Mg*)0 = 0.011±0.037 ‰
ΔtCAI = 2.24+0.59-0.37Ma
MSWD 0.42
δ26Mg* (‰)
27Al/24Mg

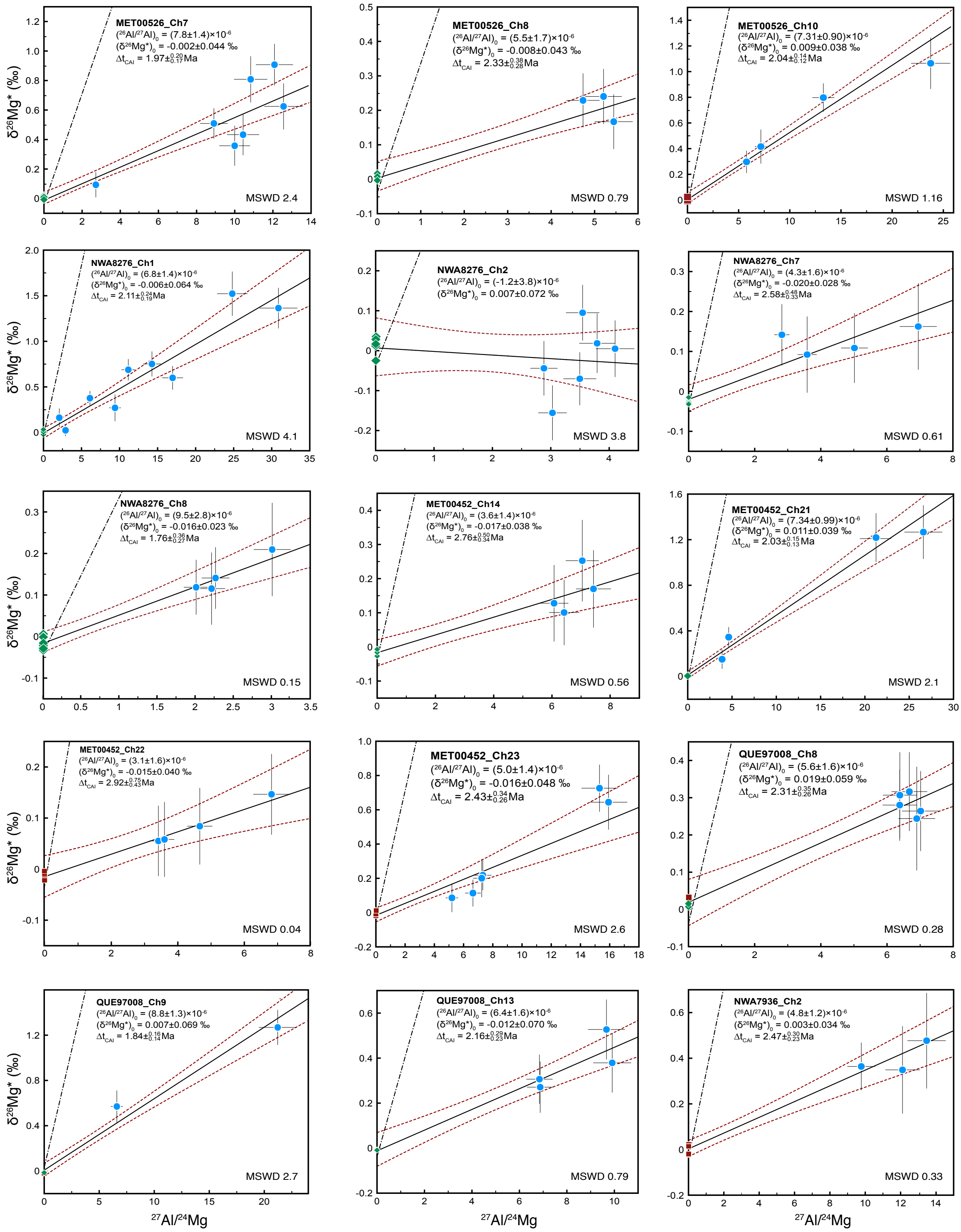

Fig. 5. Isochron diagrams for all chondrule analysed in this study. Blue circles correspond to mesostasis, green diamonds to olivine and red squares to pyroxene measurements. The dashed lines indicate $(^{26}Al/^{27}Al)_0 = 5.23 \times 10^{-5}$. Error bars are 2σ.

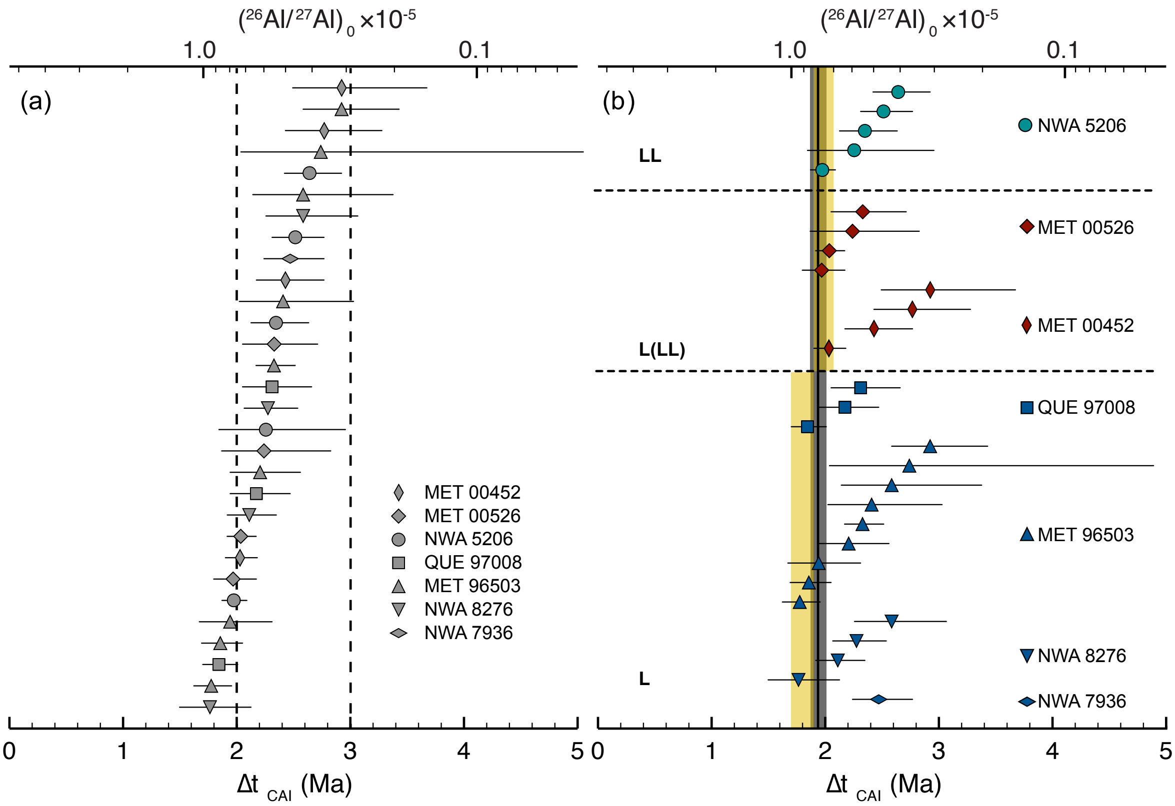

Fig. 6. ^{26}Al-^{26}Mg ages and (^{26}Al/^{27}Al)$_0$ of ordinary chondrite chondrules from this study. (a) shows the total range in (^{26}Al/^{27}Al)$_0$ and corresponding ages that is recorded by the measured chondrules. (b) the same data as shown in (a) arranged by chondrite groups and sorted by age for each sample. The yellow shaded bars mark the mean ages of the oldest chondrules in the L and L(LL)/LL chondrite samples at $1.81^{+0.11}_{-0.10}$ Ma and $1.99^{+0.08}_{-0.08}$ Ma, respectively, with their 2σ uncertainties. The solid line corresponds to the weighted mean age of $1.94^{+0.07}_{-0.06}$ for the oldest chondrules from six of the seven studied samples. Error bars are 2σ.

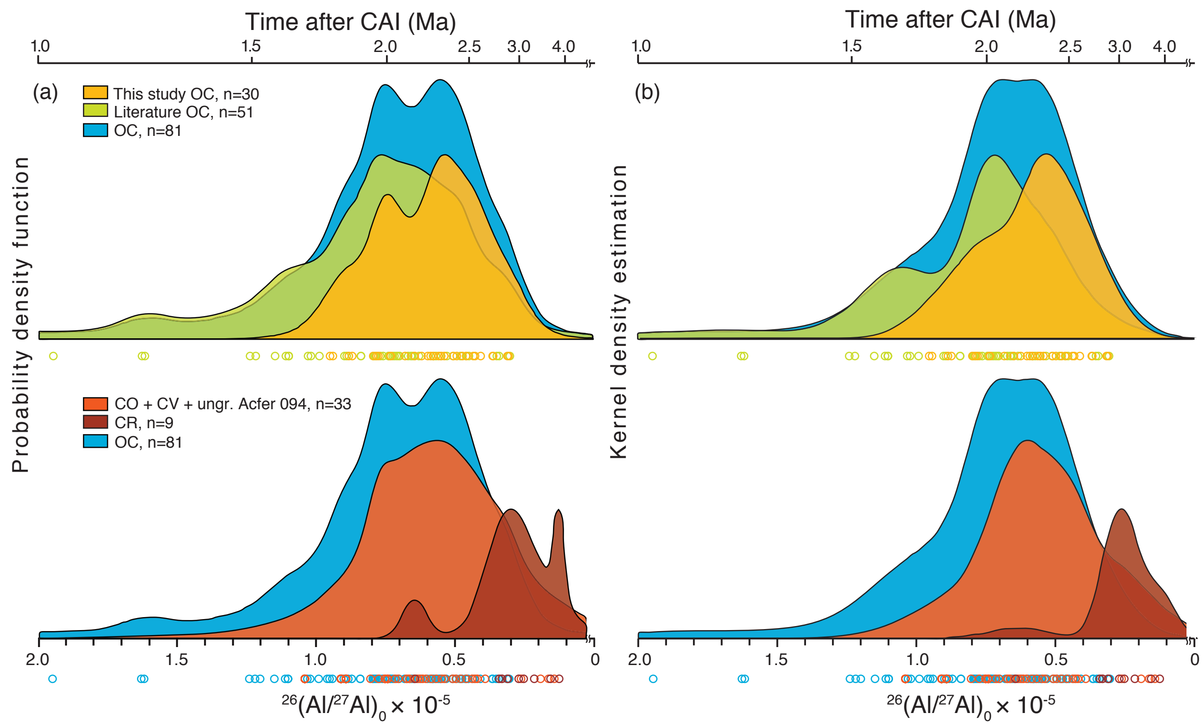

Fig. 7. a) Probability density functions (PDFs) and b) adaptive Kernel density estimates (KDE) of initial $^{26}Al/^{27}Al$ and the corresponding ^{26}Al-^{26}Mg ages of ferromagnesian chondrules from unequilibrated chondrites (petrologic type ≤3.15). The plots represent OC chondrules from this study (yellow) and literature data (green) (23 chondrules from Semarkona LL3.00 (Hutcheon and Hutchison, 1989; Kita et al., 2000; Rudraswami et al., 2008; Villeneuve et al., 2009), 13 chondrules from Bishunpur LL3.15 (Mostefaoui et al., 2002; Kita et al., 2005; Rudraswami et al., 2008), two chondrules from Y-791324 LL3.15 (Rudraswami et a., 2008) and data from Rudraswami and Goswami (2007) for Adrar 003 L/LL3.10 (2 chondrules), LEW 86134 L3.0 (3 chondrules), QUE 97008 L3.05 (4 chondrules) and LEW 86018 L3.1 (4 chondrules). Data for CCs comprise 25 chondrules from Yamato 81020 (CO3.0) (Kurahashi et al., 2008; Kunihiro et al., 2004; Yurimoto & Wasson, 2002), 12 chondrules from Acfer 094 (Sugiura & Krot, 2007; Ushikubo et al., 2010), 9 chondrules from CR2 meteorites Acfer 311, EET 92042, EET 92174, GRA 95229, GRO 03116, PCA 91082, El Djouf 001 and QUE 99177 (Nagashima et al., 2008; Nagashima et al., 2014; Schrader et al., 2017), 1 chondrule age reported by Nagashima et al. (2007) for a CR chondrite and 10 chondrules from CV3.1 Kaba meteorite (Nagashima et al., 2017). The blue areas represent the combined OC chondrule data. The orange curves represent data from literature for CO, CV meteorites and ung. Acfer 094. Data foe CR meteorites are shown in red. The circles below the plot correspond to $(^{26}Al/^{27}Al)_0$ of individual chondrules. PDFs and KDEs were calculated using DensityPlotter 8.2 (Vermeesch, 2012).